Hydraulic Conductivity Distribution from Multi-level Slug Tests and Multivariate Facies Associations in a Conglomeratic Fluvial Aquifer, Boise Hydrogeophysical Research Site

Warren Barrash[1] and Michael Cardiff[1,2]

[1] Department of Geosciences, Boise State University, Boise, ID, USA
[2] Department of Geosciences, University of Wisconsin-Madison, Madison, WI, USA

1. ABSTRACT

Knowledge of the distribution of hydraulic conductivity (K) at high-resolution in heterogeneous aquifers is important for modeling fundamental hydrologic processes, investigation and remediation of groundwater contamination, and understanding petrophysical relations or multivariate associations. We examine K structure in the conglomeratic fluvial aquifer at the Boise Hydrogeophysical Research Site (BHRS) using high-resolution K data from multi-level slug tests modeled with updated wellbore-skin K. The K data are analyzed both alone and in combination with porosity (ϕ), capacitive conductivity (CC), and grain-size distribution (GSD) data. K population pdfs (probability density functions) by ϕ-CC-lithologic stratigraphic units follow the well-established BHRS stratigraphy only in the lower half of the section, but have different rank order of relative magnitude compared with ϕ and CC. MANOVA verifies the presence of seven multivariate K-facies including one repeated type, and t-tests for K alone recognize six univariate K-facies, with two of the seven multivariate K-facies (distinguished largely by CC differences) combined into one type of univariate K facies. Cross-plots indicate K-facies exhibit multivariate parameter associations rather than correlations or petrophysical relations. Principal component analysis of K parameters with ϕ and CC (4-way), and also with GSD information (8-way), indicate nearly half the variance is related to ϕ and CC, with little influence from K. Significant fractions of the remaining variance are "flow related," with K and ϕ both varying together and in opposition. Such K-ϕ "polarity" explains the stratigraphic division of K-facies into three lower facies with K-ϕ generally varying together, and three upper K-facies with K-ϕ generally varying in opposition. GSD information indicates K variation occurs by a range of combinations of ϕ with cobble and matrix fractions, representative grain size parameters, and sorting.

2. INTRODUCTION

Determination of the distribution of hydraulic conductivity (K) at high-resolution in heterogeneous aquifers is important for modeling fundamental hydrologic processes and for investigation and remediation of groundwater contamination. Also, knowledge of the distribution of K along with other physical, geophysical, and geologic parameters (e.g., porosity [ϕ], electrical conductivity, grain size distribution [GSD]) can support understanding of the basis for K magnitudes in the field, understanding of spatial structure of K at multiple scales, and finding proxy parameters or petrophysical relations to estimate K from other kinds of measurements that may be easier and more economical to collect [e.g., Beres et al, 1999; Bayer et al., 2011; Hubbard et al., 2001; Slater et al., 2011].

Coarse fluvial and glaciofluvial deposits (e.g., Figure 1) are a class of widespread heterogeneous aquifers that have importance for fluid movement associated with water supply, numerous engineering applications, river ecology, and climate-change processes - especially in glacial melt regions. Such aquifers have been studied previously for high-resolution K distribution, but most of the K values for these investigations have been determined from lab-scale measurements (commonly on reconstructed samples) and empirical estimates based on samples from quarry and outcrop exposures [e.g., Jussel et al., 1994; Klingbeil et al., 1999; Heinz et al., 2003; Lunt et al., 2004; Zappa et al., 2006]. In these studies, K assignments are generally based on lithofacies and sedimentary facies associations. However, to date there have been few high-resolution studies with abundant in-situ K measurements in actual coarse, conglomeratic, fluvial or glaciofluvial aquifers.

Here we examine a high-resolution K data set from multi-level slug tests taken in a coarse fluvial aquifer; for this report the K data set was modeled using a revised wellbore-skin K value compared with Malama et al. [2011] and Cardiff et al. [2011] (see Section 4.1 below). A total of 518 intervals were tested (at 0.3 m offsets) in 13 fully screened wells in the central area of the Boise Hydrogeophysical Research Site, or BHRS (Figure 2). Previous work shows there is not a strong relation of K with ϕ [Cardiff et al., 2011]. But the BHRS provides the opportunity to examine the in-situ, high-resolution, K distribution in conjunction with supporting information at similar scale such as: (1) ϕ data from neutron logs [Barrash and Clemo, 2002]; (2) electrical conductivity data from capacitive conductivity (CC) logs [Mwenifumbo et al., 2009]; and (3) GSD data from core [Reboulet and Barrash, 2003; Barrash and Reboulet, 2004]. Also, K results from slug tests are consistent with 3D hydraulic tomography K results for BHRS slug-test locations [Cardiff et al., 2012; in review].

2.1 Objectives

Objectives of this study are to: (1) determine K spatial distribution and structure with respect to both the conglomeratic aquifer as a whole and to stratigraphic units recognized with ϕ, CC, and lithology in the aquifer at the BHRS; (2) recognize stratigraphic subdivisions or facies for K alone, and as multivariate K-facies together with ϕ, CC, and lithology; and (3) recognize systematics of occurrences of K, ϕ, CC, and grain size parameters to explain multivariate parameter associations or petrophysical relations with K – and thereby point to approaches for less-invasive methods to estimate K distribution and structure in coarse, conglomeratic aquifers.

2.2 Organization and Methods

Below we first present the hydrogeologic setting and the K data set for the aquifer under study. Given the prior information that K has limited correlation with ϕ and with the well-documented ϕ-CC stratigraphy at the BHRS, we address the three objectives listed above with a sequence of exploratory steps including semi-quantitative observational evidence and quantitative statistical tests. The general progression of steps (Table 1) is: (1) check the degree and nature of K organization at the ϕ-CC unit scale; (2) conduct semi-quantitative reconnaissance for presence, scale, and associations of coherent bodies or facies; (3) statistically test for differences between identified multivariate and univariate K facies, and check whether multivariate identities are due to petrophysical relations or to parameter associations; and (4) add information from GSD data to help explain the basis for differences between facies, and for parameter associations within facies. Following these analyses we compare the K distribution and relations to similar deposits in the literature, and give follow-up recommendations.

3. HYDROGEOLOGIC SETTING

The hydrogeologic setting for this study is the shallow unconfined aquifer at the BHRS which consists of ~20 m thickness of mixed cobble, gravel, and sand fluvial deposits overlying a clay aquitard. The BHRS is a research wellfield [Barrash et al., 1999] located on a gravel bar adjacent to the Boise River 15 km southeast of downtown Boise, Idaho (Figure 2). Eighteen wells were cored and screened through the unconsolidated, cobble-and-sand fluvial deposits and completed into the underlying clay. The wells were advanced with the core-drill-drive method to minimize the disturbed volume of formation outside the wells [Morin et al., 1988; Barrash et al., 2006]; with this method the formation was allowed to collapse against the slotted casing upon withdrawal of the drive casing, and no gravel pack was installed. Of the 18 wells, 13 wells are

arranged in two concentric rings (the B and C wells) around a central well (A1) in the 20-m diameter central area of the BHRS, and are surrounded by an outer ring of five "boundary" wells (the X wells) (Figure 2).

Stratigraphy at the BHRS has been principally defined with neutron ϕ logs, CC logs, and core analysis. Details on ϕ and CC logging and analysis are given in Barrash and Clemo [2002] and Mwenifumbo et al. [2009] respectively, and details on core collection and analysis are given in Reboulet and Barrash [2003] and Barrash and Reboulet [2004]. For perspective, the porosity log data set consists of measurements taken every 0.06 m with volume of investigation of approximately 0.3 m diameter. Core samples were collected in a split spoon with 0.054 m mouth and 0.6 m length. Recovery of cored length was ~82%; all samples were assigned elevation based on position relative to spoon mouth, so some positioning error occurs for some samples from partial spoons. Little mixing occurred during core sampling, but large cobbles were truncated on passage through the mouth creating a size bias for large cobbles [Barrash and Reboulet, 2004]. CC measurements were collected every 0.023 m and have a volume of investigation of about 0.3 m diameter; measurement differences are little influenced by the fluid conductivity which is nearly constant at the BHRS [Hausrath et al., 2002; Mwenifumbo et al., 2009].

The stratigraphic sequence at the BHRS includes four cobble-dominated units (Units 1-4, with unit numbers following depositional sequence from lower to higher), which are overlain by a sand channel (Unit 5) that thickens toward the Boise River and pinches out in the center of the well field. These coarse sediments are underlain by a red clay everywhere at the well field, and by a thin ($\leq$1.5 m thick) edge of a basalt flow that occurs between the clay and the coarse sediments in portions of the site. Units 1 and 3 have relatively low average ϕ and low ϕ

variance; Units 2 and 4 have higher average ϕ and higher ϕ variance; and the Unit 5 sand deposit is the highest ϕ unit [Barrash and Clemo, 2002].

Surveys using GPR, or ground-penetrating radar [e.g., Clement et al., 2006; Dafflon et al., 2011], seismic [e.g., Moret et al., 2006], and electrical resistivity methods [Slater et al., 2011] have recognized a similar distribution of stratigraphic units suggesting that geophysical responses are largely consistent with observed ϕ. However, Unit 2 has been further divided into two subunits, Units 2A and 2B (Figure 3), based on differing electrical responses identified with CC logs [Mwenifumbo et al., 2009], and on "anomalous" GPR responses in cross-well tomography [Irving et al., 2007; Ernst et al., 2007; Dafflon et al., 2011]. In addition, the presence of distinct patches and lenses within individual stratigraphic layers (e.g., Unit 4) indicate multi-scale heterogeneity beyond the larger-scale unit delineations [Barrash and Clemo, 2002].

4 HYDRAULIC CONDUCTIVITY AT THE BHRS

Recent testing at the BHRS with multi-level slug tests and the emerging method of 3D transient hydraulic tomography (3D THT) are providing high-resolution results on the heterogeneous distribution of K. Average values extracted from these methods also fall within the range of average values found with homogeneous or layer-averaged methods (Table 2). In this section we present facts on the acquisition, modeling, and overall population results of the multi-level slug tests, including use of 3D THT results for comparison.

4.1 Multi-level Slug Tests

High-resolution, high-quality, in-situ data were collected for K analysis by performing multi-level slug tests in 2008-2009. Compressed air was used to depress water levels in isolated 0.3 m intervals (with 0.6 m-long packers on either side). Tests were run at two or three different slug heights per zone, and commonly were repeated [e.g., Butler, 1998]. Details of data collection, modeling analysis, data quality, and information content are given in Malama et al. [2011] and Cardiff et al. [2011]. Overall, 741 intervals were tested in the 18 wells at the BHRS; here we examine 518 of those intervals in the sedimentary aquifer from the 13 wells in the central area where wells are in close proximity (Figure 2) and there is a high density of independent testing data for support and comparison.

Previously published K results from these multi-level slug tests [Cardiff et al., 2011; Malama et al., 2011] were analyzed with estimated bounds for wellbore-skin K at the BHRS of: (1) the aquifer K (upper bound, i.e., no skin); and (2) 2×10^{-4} m/s (lower bound, which is 10 times higher than the estimated wellbore skin from the pumping test analyses of Barrash et al., 2006). The presence of positive wellbore skin is clear from "excessive" drawdown observed at pumping wells relative to observation wells (e.g., Figure 3 in Barrash et al. [2006]). However, initial modeling results with skin K of 2×10^{-4} m/s gave anomalously high- to very high-K values from slug tests toward the high end of results [Cardiff et al., 2011], which suggested that a larger wellbore-skin K value at the BHRS would be appropriate. The slug K data set analyzed in this paper has been generated using wellbore-skin $K = 5 \times 10^{-4}$ m/s (Figure 4). Subsequently available information from hydraulic tomography at the BHRS [Cardiff et al., in review] provides high-resolution comparison data at well locations which are consistent with K values from slug tests modeled here using a wellbore-skin K value of 5×10^{-4} m/s.

4.2. K Population Facts

Here we present basic facts about the K (or log10K and lnK) population at the BHRS for perspective before looking for more detailed structure and multivariate associations. The overall log10K mean is -3.045 m/s and variance is 0.093 m^2/s^2 for all slug tests in the coarse fluvial aquifer in the 13 wells in the central area of the BHRS (Table 3A). Although the average K is higher than most other field methods used for estimating K at the BHRS by up to half an order of magnitude (Table 2), we note that the difference is similar to, or considerably smaller than, differences between multiple field methods reported in other published high-resolution studies in unconsolidated sedimentary aquifers [e.g., Zlotnik et al., 2000; Alexander et al., 2011]. Also we note that the lnK variance is 0.49 which indicates the BHRS has low to perhaps moderate heterogeneity in relation to other well-studied unconsolidated sedimentary aquifers. For example, Cape Cod (lnK variance of 0.14, Wolf, 1988) and Borden (lnK variance of 0.3, Sudicky et al., 1986) have low heterogeneity, and the MADE site (lnK variance of 4.5, Rehfeldt et al., 1992) has very high heterogeneity. Geostatistical structure of K at the BHRS can be modeled as an exponential structure having lateral correlation lengths of x = 5.9 m and y = 4.3 m and vertical correlation length of 1.2 m, which are similar to values reported in Cardiff et al. [2011], and in Barrash and Clemo [2002] for porosity.

5. COMPARISONS OF K, ϕ, AND CC FOR STRATIGRAPHIC UNITS

Given the success of the ϕ-CC stratigraphy paradigm at the BHRS (described in Section 3 above), we first consider whether the log10K population is also organized into subdivisions coincident with ϕ and CC stratigraphic units. Note: we do not include Unit 5 in this analysis

because of the fundamental difference in material type (i.e., sand of Unit 5 vs mixed cobbles, gravels, and sand of Units 1-4).

First we check to what degree, if any, log10K subpopulations have pdfs or histograms that are similar to ϕ subpopulations based on recognized ϕ and CC stratigraphy. Figure 5 presents a unit-by-unit comparison of histograms or pdfs for log10K and ϕ, and shows that log10K pdfs in cobble-dominated units (Units 1-4) have somewhat Gaussian distributions with positive skewness, as do ϕ pdfs. Also it is apparent that the relative magnitudes of log10K and ϕ do not always trend together for vertically adjacent units (i.e., Unit 1 is less than Unit 2A for both log10K and ϕ, but Unit 2A log10K is less than Unit 2B log10K while Unit 2A ϕ is greater than Unit 2B ϕ - see Table 3, Figure 5).

Next we check if vertically adjacent log10K subpopulations (by ϕ-CC stratigraphic unit) are statistically different from each other. Some of the log10K subpopulation pdfs (Figure 5) are not obviously distinct so we conducted t-tests on vertically adjacent log10K subpopulations for two sequences: one including Unit 2B and one without Unit 2B (Table 3B). Here the results differ from findings for ϕ units in that three of the log10K subpopulations in vertically adjacent ϕ units are not statistically distinguishable (Units 4, 3, 2A). That is, organization of log10K subpopulations by ϕ-CC unit stratigraphy may be recognized in the lower half of the section, but ϕ influence on log10K magnitude differs between at least Units 2A and 2B. And distinctions between Units 3 and 4 that are apparent for ϕ and CC, are not apparent for log10K.

6. K STRUCTURE INDEPENDENT OF POROSITY

Given mixed results for identifying first-order K or log10K association with ϕ or CC, we next "step back" and consider log10K spatial occurrence alone, because some local K coherence

is evident within and between wells (Figures 4 and 6 here, and Cardiff et al. [2011]). We apply

5-pt moving-average filters to well profiles of log10K and standard deviation of log10K as

screening tools for recognizing local intervals within and between adjacent wells that have

similar K mean and standard deviation, but which differ from intervals above and below (Figure

6). Such criteria are commonly used for recognizing different distinct subpopulations or bodies

[e.g., Journel and Huijbregts, 1978; Barrash and Reboulet, 2004].

Indeed it appears that log10K occurrence is not completely unstructured but rather: (1)

some log10K bodies with local lateral continuity can be recognized by observation in this

manner; and (2) contacts between local log10K bodies commonly occur at known ϕ-CC unit

boundaries or sedimentary contacts (Figure 6). However, while this method provides semi-

quantitative support for the presence of K lenses or facies at the subunit scale, it may not be

possible or practical to use this method for complete and certain identification of these bodies.

And our experience with unit-identification algorithms is largely similar in that clearly distinct

units can be identified with confidence, but local ambiguity is common and difficult to

overcome.

7. WELL LOG COMPARISON FOR SUBUNIT K, ϕ, AND CC STRUCTURE

To continue the effort to recognize K structure in the coarse fluvial aquifer at the BHRS,

we plot and compare individual well profiles of log10K, standard deviation log10K, ϕ, and CC.

To facilitate both plotting of different parameters together and later using multivariate statistics,

we: (1) generate ϕ and CC logs at wells with parameter values at similar moving-average length

intervals (0.3 m); (2) extract the moving average ϕ and CC measurements at locations of log10K

measurements; and (3) transform the populations of log10K, standard deviation log10K, ϕ, and

CC to respective normalized populations of zero mean and unit variance. To illustrate the types of parameter associations that occur in locally coherent bodies within and between wells, examples are given in Figure 7 for two pairs of two adjacent wells (B6 and C5, and B3 and C2) in the central area of the BHRS.

7.1 Plots of Transformed Parameters

Plots of transformed log10K, ϕ, and CC together by well (Figure 7) show: (1) local segment and sequence coherence within and between wells; (2) local K "subunit" breaks that commonly occur at ϕ-CC unit breaks; (3) some subunits recognized in the plots here (Figure 7) are similar to those recognized with 5-pt moving average plots of log10K and standard deviation log10K (Figure 6); and (4) although local K subunit breaks commonly occur at ϕ subunit breaks, these plots show that the type of association between log10K and ϕ subunits is not unique with respect to positive or negative correlation, or with respect to relative or absolute magnitude. That is, ϕ and CC vary alone or together in K lenses or facies where log10K and standard deviation log10K vary together, but not always with the same magnitude sense or polarity.

As seen in the four example wells in Figure 7, several types of local variation occur generally on the scale of 1-3 m vertically and either within a given well alone or within adjacent wells at the same elevation, suggesting that some degree of lateral continuity is common. Several such types are:

(1) Very high K with very low CC and moderate ϕ (Unit 2B at about 838-840 m elevation in wells B6 and C5 – see lenses circled in black in Figure 7);

(2) Relatively low K with moderate-to-high ϕ and "average" CC in Units 2A and 4 (e.g., 837-838 m in wells B6 and C5; 834-836 m in wells B3 and C2 – see lenses circled in blue in Figure 7);

(3) Relatively high K with relatively low ϕ and average-to-low CC in one or more lenses, $\leq$1 m thick, in wells B3, B6, and C2 (see lenses circled in red in Figure 7);

(4) K and ϕ varying together in relatively higher or lower magnitude sense with variable CC magnitude (e.g., several lenses in Unit 4 of well B3; lenses in Unit 2A of wells B3 and C5, ~1 m thick – see lenses circled in green in Figure 7).

The local variation of lens types is consistent with the recognition that: (1) the relative magnitudes of ϕ and CC, or log10K, for Units 1-4 (Figures 3 and 5 here, and Figure 4 in Barrash and Clemo [2002]) do not hold in detail everywhere within the stratigraphic units; and (2) much of the variation within Units 1-4 may be associated with smaller-scale lenses of a variety of types, rather than with just one type of petrophysical relation or parameter association.

8. MULTIVARIATE STATISTICAL ANALYSIS OF LOG10K, STANDARD DEVIATION LOG10K, ϕ, AND CC

Given the observational evidence above for distinct K bodies, including bodies with systematic and repeated combinations of parameter associations (e.g., Figures 6-7), we continue the investigation of K-facies with multivariate methods.

8.1 Principal Component Analysis, K-Facies, and Multivariate Associations or Petrophysical Relations

We conduct a 4-way principal component analysis (PCA) to find multivariate K-facies using the transformed population values for log10K, standard deviation log10K, ϕ, and CC at co-located positions in 13 BHRS central area wells. Results (Figure 8, Table S1) clearly show little association of log10K and standard deviation log10K with ϕ (plus or minus CC) in apportioning variance. That is, the major PCs have either: (1) similar dominant amounts of ϕ and CC with average log10K and standard deviation log10K (PC4 or "ϕ-CC" PC, with 39.4% of the total variance), or (2) similar dominant amounts of log10K and standard deviation log10K with average ϕ, and minor CC in opposition to the log10K and standard deviation log10K (PC3 or "K-K variability" PC, with 31.8% of total variance). PC2, or "K-anti-K variability" PC, accounts for 20.2% or an intermediate amount of the variance and has similar contribution magnitudes from log10K and standard deviation log10K - but they are in opposition (i.e., high log10K associated with low standard deviation log10K, and vice versa), and again only average amounts of ϕ and CC. PC1, or "Porosity-anti-CC" PC, accounts for 8.4% of the variance with significant contributions from porosity and CC in opposition, but limited contributions from log10K and standard deviation log10K.

8.2 Multivariate K-Facies Recognized in Well Profiles of PC Scores and Transformed Log10K

To continue, we calculate PC scores and plot these scores by well as vertical profiles to search for coherent bodies and possible insight into the multivariate basis for parameter associations [e.g., Davis, 1986; Barrash and Morin, 1997]. Figure 9 shows example plots of scores at four wells for PCs 4 and 3 (which together account for 71.2% of the total variance) along with transformed log10K for reference (e.g., note PCs 4 and 3 are plotted *(-1) to give

more intuitive relative behavior with the log10K profile). Several types of multivariate bodies, or K-facies, are identified in vertical sequences within wells and between wells (Figure 9):

(1) K-Facies D: Very high –PC3 (dominantly log10K and standard deviation log10K) with low –PC4 (ϕ and CC) in Unit 2B at 838-841m elevation in wells B6 and C5;

(2) K-facies E and F: Moderate to locally high –PC3 with lowest –PC4, defining all or nearly all of Unit 3 within the elevation range of 838-842 m in wells B3 and C2; somewhat similar bodies identified as K-facies F occur in Unit 4 of wells B6 and C5;

(3) K-facies C and B: Relatively low –PC3 with moderately high –PC4 within the elevation range of 836.5-838 m (i.e., the upper portion of Unit 2A) in all four example wells, and with repeated occurrence of the relatively low –PC3 with moderately high –PC4 multivariate behavior (identified as multivariate K-facies B) in wells B3 and C2 in the interval 834-836 m, or the lower portion of Unit 2A;

(4) K-facies G: Perhaps somewhat similar to K-facies C of (3) above, with low-to-moderate –PC3 and high –PC4 in the lower part of Unit 4 at 842.5-844 m in wells B3 and C2.

Based on the PCA analysis and initial review of profile plots of PC scores for systematic occurrences of K bodies or lenses, we note that several types of combined PC associations have repeated occurrences at similar intervals in adjacent wells (Figure 9, Table 4), including intervals that break at or very near ϕ–CC unit contacts (e.g., (1)-(4) above). Also, not all locations in the logs of –PC4 and –PC3 scores are easily assigned to coherent and repeated bodies; these apparently less-structured regions are addressed below.

9. OCCURRENCE, STATISTICAL ASSESSMENT, AND MEANING ASSESSMENT OF MULTIVARIATE K-FACIES

While the analyses above indicate that K-facies can be recognized from transformed well records of log10K, standard deviation log10K, ϕ, and CC, it may be difficult to completely characterize well profiles in this way without some ambiguity and subjectivity. However, it may be possible to interpret or hypothesize meaning and spatial distribution for K-facies at the BHRS which then may be tested statistically here, and tested subsequently with independent field methods at the BHRS or elsewhere. The question of whether the basis for multivariate behavior in K-facies is either petrophysical (i.e., functional) relations or parameter associations (consistent "average" tendencies as in a cluster sense) is then considered with cross-plots of the main parameters.

9.1 Occurrence of Multivariate K-Facies

Continuing in this direction, we identify and describe eight multivariate K-facies from observation of PC score logs where a given facies occurs at approximately the same elevation interval in three or more adjacent wells (Table 4, Figure 9). K spatial distribution and structure outside these bodies may occur as a next-larger-scale "host" material (e.g., as in "mixed layers of grey and brown gravels" in Jussel et al. [1994]), where the "host" surrounds the next-smaller-scale distributed lenses of K-facies identified here.

Three other aspects of the multivariate K-facies occurrence are systematic and so deserve mention: (1) the K-facies occur within (or, in the case of K-facies A, are coextensive with) ϕ-CC stratigraphic units (Table 4), with minor overlap exceptions; (2) the vertical sequence of K-facies follows a progression from lower K to higher K to lower K (Table 4, and consistent with Figure 5); and (3) the lower portion of the sequence (K-facies A-D) has the overall association of K magnitude in positive polarity with ϕ, but the upper portion of the sequence (K-facies E-H) has

the overall association of K magnitude in negative polarity with ϕ (Table 4 here and Figure 13 in Cardiff et al. [2011]).

9.2 Statistical Assessment of Multivariate K-facies

To test if the populations of the eight multivariate K-facies are statistically different, we conduct MANOVA [e.g., Johnson and Wichern, 1998] between vertically adjacent K-facies and between K-facies and the "host" material at the elevation interval of a given K-facies. Results in Table 5 show that all such distinctions, except between multivariate K-facies B and C, are statistically significant. Recognizing this similarity of B and C, these two bodies are now identified as repeated occurrences of a single facies type: K-facies BC (Table 4, Figure 9).

9.3. Cross-plots to Check for Petrophysical Relations or Parameter Associations

Cross-plots provide a visual assessment of correlation or functional relations between parameters; the visual assessment can be followed with statistical tests or modeling if a relation is apparent. We have generated cross-plots between log10K and ϕ, ϕ and CC, and log10K and CC for each of the multivariate K-facies and the host material surrounding them. Figure 10 shows representative examples from three K-facies. The cross-plot clouds suggest that the identities of K-facies are due to parameter associations, in the sense of similar mean tendencies, rather than due to correlation or functional (i.e., petrophysical) relations.

9.4. T-Tests to Check for K Differences between Multivariate K-facies

Although seven multivariate K-facies have been identified, validated statistically, and traced laterally and vertically (Figure 11, Tables 4-5), a question remains as to whether the

differences between facies always include statistically significant differences in K. That is, while it was valuable to use a multivariate investigative approach to find distinctive bodies that include K for their identities, to estimate K structure and distribution it is now important to determine which multivariate K-facies are also distinct from adjacent facies and hosts on the basis of K alone. Results from K-population t-tests for adjacent facies and hosts (Table 6) show that all multivariate facies distinctions hold also for K except for the distinctions between facies E and F (now combined as univariate K-facies EF), and between facies E and host at the elevation interval of facies E.

10. CAN INCLUSION OF GSD INFORMATION IMPROVE UNDERSTANDING OF THE BASIS FOR MULTIVARIATE K-FACIES?

Now we consider whether inclusion of GSD data can help explain the basis for K magnitude variations and facies associations. Extensive GSD data are available from core at the BHRS, but a number of facts need to be stated for perspective in their use [Reboulet and Barrash, 2003; Barrash and Reboulet, 2004]: (1) core recovery of the coarse, unconsolidated sediments is high, but incomplete (i.e., ~82% of full well depths were recovered); (2) elevation positioning has uncertainty for samples collected in incompletely filled core barrels; (3) large cobbles were truncated upon entry through the 5.4-cm-diameter barrel mouth; (4) complete recovery of all constituents for a given sample cannot be assured, although vertical mixing in the core sample column is minimal; and (5) sample lengths of lithotypes in core are variable between 0.075 m and 0.3 m. A consequence of the incomplete core recovery is a corresponding reduction in the density of collocated data that can be used from other parameters (i.e., log10K, ϕ, CC) for multivariate analysis with GSD information.

10.1 8-Way PCA with GSD Parameters

We use 8-way PCA with five GSD parameters plus log10K, CC, and ϕ assigned to the matrix volume (i.e., a ϕ-metric that is more relevant to K than full-sample ϕ because fluid flow occurs in the pores in the matrix between the "framework" cobbles). The five GSD parameters are: (1) d60 for the full distribution (measure of cobble size); (2) d60/d10 for the full distribution (sorting for the whole sample); (3) d10 of the matrix (representative grain size for the portion of the sample where flow occurs); (4) d60/d10 of the matrix (sorting of the portion of the sample where flow occurs); and (5) solid volume percent due to cobbles (cobble : matrix proportion). For this analysis, "cobbles" are defined as grains >9.525 mm, and "matrix" is defined as grains >.0625mm to 9.525 mm; the BHRS sediments have negligible silt or clay [Reboulet and Barrash, 2003].

PCA was initially run on the full-sample data set of multivariate K-facies (Figure 12, Table S3). Heuristic assessment of the four largest PCs (comprising 81.9% of total variance) is similar to that for 4-way PCA whereby: (1) a significant fraction of the variance is due to physical and electrical variability that is "K-neutral" (PC8 with 43.2% of the variance); and (2) a comparable, significant fraction of the total variance is due to factors influencing flow behavior (i.e., larger K contribution in PCs 7, 6, and 5 with combined variance of 40.7%). Inclusion of the additional GSD parameters can add insight into parameter combinations and polarities that contribute to K magnitudes associated with the different K-facies – but this is difficult to discern from the full sample set. So, next we run PCA on a facies-by-facies basis (Tables S4-S9, Figures S1-S6).

10.2 Interpretation of GSD Meaning for K Variation in K-Facies from 8-way PCA

Results in terms of parameter loadings, by K-facies, on the most important "K" PCs (PCs 7, 6, and 5) are given in Table 7. Two reasons that suggest the identified systematics in Table 7 have meaning are: (1) repeated occurrence of five important "K" PCs (denoted by color coding in the top "facies-PC" row); and (2) consistency among types of facies where repeated PCs occur (i.e., three occur only among the stratigraphically lower group of facies with positive K-ϕ polarity, and two occur only among the stratigraphically higher group of facies with opposite K-ϕ polarity).

Insight into GSD influence on K can be extracted from Table 7 by noting the combinations of parameters with common positive and negative signs, or polarities, associated with increased K PC loading. Information from Table 7 is plotted in Figure 13 to help identify GSD influence as parameter combinations and trends. In this regard, Figures 13A-C show no trend (but considerable variability) in GSD parameters or matrix-ϕ with increasing log10K in PCs of Table 7 that have significant K loading. This is consistent with the problematic nature of defining the basis for K in these conglomeratic sediments: *local combinations of parameters are more important in determining K than a single proxy parameter, or a single petrophysical relation.* Even so, ϕ will always be an important element of such combinations because that is where the flow occurs; but as with K, Figures 13 E-F show no consistent trends with ϕ, although again the local parameter details provide meaningful context.

That is, while no loading parameters trend consistently with increasing K or increasing ϕ, considerable numbers of parameters appear to *vary together, either positively or negatively, for low and high segments of the K or ϕ ranges* (Figure 13, Table 8). For due diligence, we run correlation statistics on parameter pairs with apparently similar positive or negative tracking

20

behavior, and we note that the correlation coefficients suggest moderate-to-strong relations – although only four of 18 pairs are statistically significant at the 0.05 level. However, sample numbers are small (Table 8), and lack of significance does not necessarily mean that no correlations exist. In this regard, we continue the analysis with the reasonable presumptions that some, or all, of the apparent correlations: (1) have physical basis; and (2) provide working hypotheses to test in the future with additional in-situ data from similar conglomeratic aquifers. For example, the role of cobbles (e.g., cobble size, sorting, and volume percent of a given sample) exhibit important relations with K and ϕ (Table 8) despite relatively minor magnitude ranges (Figures 13A and 13E).

Furthermore, systematics of covariation with CC (Table 8, Figures 13C and 13F) appear to include: (1) positive correlation with ϕ for the low-medium K segment of the K range; (2) perhaps negative correlation with ϕ for the high-K segment of the K range; (3) negative correlation with K for the high-ϕ segment of matrix-ϕ range; and (4) increasing CC with progressively better sorting of the sample as a whole (d60/d10-all). Also, for three cases, relatively limited magnitude ranges of a given parameter, rather than correlation or trending with one or more other parameters, is diagnostic for a given segment of the K or matrix-ϕ ranges. In particular: (1) poorer matrix sorting (i.e., higher ratio of d60/d10-matrix) occurs in the low-K segment (Figure 13B); (2) relatively small-to-average matrix d10 occurs in the high-K segment (Figure 13B); and (3) high matrix d10 occurs in the high matrix-ϕ segment (Figure 13E).

10.3 GSD Association with K-ϕ Opposite Polarity in K-Facies

Different combinations of GSD metrics associated with K-facies showing positive and negative association of K with matrix-ϕ can be seen by reviewing PCs in Table 7. For example,

21

PCs with *opposite loadings of K and matrix-ϕ* in K-facies A (PC6), BC (PC7), EF (PC6), G (PC 6), and H (PC6) consistently have better matrix sorting (i.e., lower ratio of d60/d10-matrix) and lower volume percent of cobbles (Figures S1-S2 and S4-S6, respectively). However, PCs with *same-sign loadings of K and matrix-ϕ* in K-facies A (PC7), BC (PC5), EF (PC7), and H (PC7) have larger d10-matrix and better whole-sample sorting (Figures S1-S2, S4 and S6, respectively) – which are different GSD metrics that are consistent contributors to higher K, in addition to higher matrix-ϕ. That is, it appears that several GSD parameter metrics occur consistently in K-facies that have opposite (i.e., positive and negative) polarity of K with ϕ, although not all GSD metrics occur consistently in similar relative proportions for the opposite K and matrix-ϕ facies associations.

11 COMPARISON WITH PUBLISHED K MAGNITUDES AND DISTRIBUTIONS IN SIMILAR DEPOSITS

Lunt et al. [2004] pointedly note a "paucity of accurate published data on K in gravelly fluvial deposits" after presenting new data and surveying recent literature on studies of sediments similar to those in the unconfined aquifer at the BHRS. Nearly all the K data in the literature on similar deposits are taken from reconstructed lab samples and empirical estimates based on assumed Kozeny-Carman petrophysics using samples from quarries and outcrops [e.g., Jussel et al., 1994; Klingbeil et al., 1999; Heinz et al., 2003; Lunt et al., 2004; Zappa et al., 2006]. The internal architectures of these very well-described deposits are similar to quarries and outcrops in the vicinity of the BHRS; the composition and sedimentary facies types are similar to reconstructions of the unconfined aquifer at the BHRS [Barrash and Clemo, 2002; Reboulet and Barrash, 2003; Barrash and Reboulet, 2004]; and K magnitudes from the large number of BHRS

slug tests are similar to previous findings (e.g., Tables 2-3 in Zappa et al. [2006] and Table 3 in Lunt et al. [2004]).

However, what appears to be different between the previous studies and work presented here (in addition to the high-density availability of collocated K, ϕ, CC, and core/GSD data) is the nature of the association of K-facies with sedimentary facies and with key parameters (ϕ, CC, GSD metrics). That is, considering the varied parameter associations detailed above, it appears that a given K population likely will not be consistently associated with a given sedimentary facies, and that the Kozeny-Carman relation assumed commonly in the literature may not be appropriate for predicting K values at the BHRS, and perhaps other sites. Other high-resolution in-situ K measurement studies in coarse conglomeratic aquifers at other sites will help determine if K-facies systematics and parameter associations interpreted at the BHRS occur elsewhere and can be quantified.

12   SUMMARY AND CONCLUSIONS

12.1   In this study we adopt an exploratory approach to search for K structure using data from multi-level slug tests (modeled with updated wellbore-skin K) at 13 wells in the central area of the BHRS. Such an approach is necessary because of: (1) the lack of strong K correlation with ϕ; and (2) the ambiguous association of K with ϕ-CC stratigraphy (Figure 5) – whereby log10K pdfs by ϕ-CC units are somewhat Gaussian and positively skewed, as are ϕ pdfs; but (3) the relative magnitude between log10K and ϕ for a number of units is different; and (4) the unit structure of the upper part of the ϕ-CC stratigraphy is not recognized in the log10K pdfs.

12.2   For the coarse conglomeratic fluvial aquifer at the BHRS, working with transformed

populations of log10K, standard deviation log10K, ϕ, and CC (i.e., transformed to zero mean and

unit variance for coincident measurements with comparable support volume) facilitated follow-

up analyses with moving average and multiple-parameter well profile plots, and with PCA and

MANOVA.

12.3   Univariate and multivariate comparison of well profiles yield consistent evidence for the

presence of K spatial structure as recognizable bodies within and/or traceable between wells

(e.g., Figures 6-7 and 9).

12.4   Multivariate statistical analysis with PCA (Figure 8) provides evidence for a division in

variance among the dominant PCs of: (1) K (log10K and standard deviation log10K – i.e., flow-

related characteristics); and (2) ϕ and CC (physical/electrical characteristics).

12.5   Profile plots or logs of PC scores at wells support identification and mapping of eight

multivariate K-facies (A-H) (Figures 9 and 11, Table 4).

12.6   The multivariate K-facies can be grouped into two types of K-ϕ parameter associations at

the BHRS (Table 4): K-ϕ associations with positive and negative polarity. K-facies by K-ϕ

polarity occur within ϕ-CC units (Table 4) and commonly terminate at ϕ-CC unit contacts.

However, not all of the aquifer sediments are assigned to these multivariate K-facies. Rather,

facies appear to be surrounded by (less locally structured) "host" sediments in a manner similar

to findings by Jussel et al. [1994] in Rhine gravel quarries.

12.7   Application of MANOVA to interpreted multivariate K-facies that are in vertical

succession (Table 5) shows that: (1) all but one of the interpreted multivariate K-facies

distinctions are statistically significant; and (2) the two interpreted K-facies that are not

statistically different (B and C) occur in the same ϕ-CC stratigraphic unit and have the same ϕ-

CC association. So, with the application of MANOVA, the number of interpreted multivariate K facies in the coarse fluvial aquifer at the BHRS is reduced from eight to seven.

12.8 Univariate log10K statistical comparisons (Table 6) support the combination of multivariate K-facies B and C, and also warrant combination of univariate K-facies E and F, and K-facies E with Host E.

12.9 The recognition and mapping of K-facies in this study lead to predictions of occurrence (Table 4, Figure 11) that are different from the established site ϕ-CC-lithology stratigraphy [Barrash and Clemo, 2002; Barrash and Reboulet, 2004; Mwenifumbo et al., 2009], but are consistent with results from independent 3D tomographic measurement and modeling at the BHRS (Figure 4 and Cardiff et al. [2012; in review]; Slater et al. [2011]).

12.10 Inclusion of GSD parameters from core in further multivariate (8-way PCA) analysis allows insight into the lithologic basis for some parameter associations. In particular, PCA with GSD parameters: (1) corroborates the earlier finding of variance split into physical PCs (minimal K influence) vs flow-related PCs (significant or dominant K influence); (2) identifies repeated occurrences of PC types among K-facies in similar association groups; and (3) identifies repeated GSD metrics for positive and negative "polarity" of K-ϕ facies associations.

12.11 Recognition of detailed systematics of GSD parameter correlation or covariation is improved with parameter loading plots by facies with increasing K and increasing ϕ (Figure 13, Table 8). These plots show that multiple parameters vary together for high and low segments of K and ϕ ranges, respectively, and do not have only monotonic relations.

12.12 Given that a number of combinations of GSD metrics along with ϕ can result in a given K (or CC) magnitude in the coarse conglomeratic aquifer at the BHRS, and to the extent that similar multiple associations or petrophysical relations likely occur in other similar aquifers,

prediction of the spatial distribution of K from ϕ and electrical conductivity will need better understanding of other GSD factors influencing K multivariate associations and/or petrophysics.

13 ACKNOWLEDGMENTS

14 REFERENCES CITED

Alexander, M., Berg, S., and Illman, W., 2011, Field study of hydrogeologic characterization methods in a heterogeneous aquifer, Ground Water, 49(3), 365-382.

Barrash, W. and Clemo, T., 2002, Hierarchical geostatistics and multifacies systems: Boise Hydrogeophysical Research Site, Boise, Idaho, Water Resources Research, 38(10), 1196, doi:10.1029/2002WR001436.

Barrash, W. and Morin, R., 1997, Recognition of units in coarse, unconsolidated braided-stream deposits from geophysical log data with principal component analysis, Geology, 25(8), 687-690.

Barrash, W. and Reboulet, E.C., 2004, Significance of porosity for stratigraphy and textural composition in subsurface coarse fluvial deposits, Boise Hydrogeophysical Research Site, Geological Society of America Bulletin, 116(9/10), 1059-1073, doi:10.1130/B25370.1.

Barrash, W., Clemo, T., Fox, J.J., and Johnson, T.C., 2006, Field, laboratory, and modeling investigation of the skin effect at wells with slotted casing, Journal of Hydrology, 326, (1-4), 181-198, doi:10.1016/j.jhydrol.2005.10.029.

Barrash, W., Clemo, T., Johnson, T., Leven, C., Malama, B., and Nelson, G., 2007, Hydraulic tomography at the Boise Hydrogeophysical Research Site, SIAM Conference on Mathematical and Computational Issues in the Geosciences, March 19-22, 2007, Santa Fe, NM.

Barrash, W., Clemo, T., and Knoll, M.D., 1999, Boise Hydrogeophysical Research Site (BHRS): Objectives, design, initial geostatistical results, Proceedings of SAGEEP99, The Symposium on the Application of Geophysics to Engineering and Environmental Problems, March 14-18, 1999, Oakland, CA, p. 389-398.

Bayer, P., Huggenberger, P., Renard, P., and Comunian, A., 2011, Three-dimensional high resolution fluvio-glacial aquifer analog: Part 1: Field study, Journal of Hydrology, 405, 1-9.

Beres, M., Huggenberger, P., Green, A.G., and Horstmeyer, H., 1999, Using two and three-dimensional georadar methods to characterize glaciofluvial architecture, Sedimentary Geology, 129, 1–24.

Butler, J.J., 1998, The design, performance, and analysis of slug tests, Lewis Publishers, Boca Raton, FL., 252 p.

Cardiff, M., Barrash, W., and Kitanidis, P., 2012, A field proof-of-concept of aquifer imaging using 3D transient hydraulic tomography with temporarily-emplaced equipment, Water Resources Research, 48, W05531, doi:10.1029/2011WR011704.

Cardiff, M., Barrash, W., and Kitanidis, P., in review, Resolution of hydraulic conductivity imaging from 3-D transient hydraulic tomography at several pumping/observation densities, submitted to Water Resources Research.

Cardiff, M., Barrash, W., Kitanidis, P., Malama, B., Revil, A., Straface, S., and Rizzo, E., 2009, A potential-based inversion of unconfined steady-state hydrologic tomography, Ground Water, 47(2), 259-270, doi: 10.1111/j.1745-6584.2008.00541.x.

Cardiff, M., Barrash, W., Thoma, M., and Malama, B., 2011, Information content of slug tests for estimating hydraulic properties in realistic, high-conductivity aquifer scenarios, Journal of Hydrology, 403(1-2), 66-82.

Clement, W.P., Barrash, W., and Knoll, M.D., 2006, Reflectivity modeling of ground penetrating radar, Geophysics, 71(3), K59-K66, 10.1190/1.2194528.

Clemo, T., 2007, MODFLOW-2005 Ground-Water Model User Guide to the Adjoint State Based Sensitivity Process (ADJ), Technical Report BSU CGISS 07-01, Center for Geophysical Investigation of the Shallow Subsurface, Boise State University, 45 p.

Dafflon, B., Irving, J., and Barrash, W., 2011, Inversion of multiple intersecting high resolution crosshole GPR profiles for hydrological characterization at the Boise Hydrogeophysical Research Site, Journal of Applied Geophysics, 73(4), 305-314.

Davis, J.C., 1986, Statistics and data analysis in geology, New York, John Wiley & Sons, 646 p.

Ernst, J., Green, A., Maurer, H., and Holliger, K., 2007, Application of a new 2D time-domain full waveform inversion scheme to crosshole radar data, Geophysics, 72, J53-J64.

Fox, J.J., 2006, Analytical modeling of fully penetrating pumping tests at the Boise Hydrogeophysical Research Site for aquifer parameters and wellbore skin, M.S. Thesis, Boise State University, Boise, ID, 132 p.

Hausrath, E.M., Barrash, W. and Reboulet, E.C., 2002, ,Water sampling and analysis for the Tracer/Time-Lapse Radar Imaging Test at the Boise Hydrogeophysical Research Site: Center for Geophysical Investigation of the Shallow Subsurface Technical Report BSU CGISS 02-02,

Boise State University, Boise, ID, 86 p.

Heinz, J., Kleineidem, S., Teutsch, G., and Aigner, T., 2003, Heterogeneity patterns of Quaternary glaciofluvial gravel bodies (SW-Germany): Application to hydrogeology, Sedimentary Geology, 158(1-2), 1-23.

Hubbard, S., Chen, J., Peterson, J., Majer, E., Williams, K., Swift, B., Mailloux, B., and Rubin, Y., 2001, Hydrogeological characterization of the South Oyster bacterial transport site using geophysical data, Water Resources Research, 37(10), p. 2431-2456.

Irving, J., Knoll, M., and Knight, R., 2007, Improving radar velocity tomograms: A new approach to incorporating high-angle traveltime data, Geophysics, 72, J31-41.

Johnson, R.A. and Wichern, D.W., 1998, Applied multivariate statistical analysis (4th ed.), Upper Saddle River, NJ, Prentice Hall, 816 p.

Journel, A.G. and Huijbregts, C.J., 1978, Mining geostatistics, San Diego, Academic Press, 600 p.

Jussel, P., Stauffer, F., and Dracos, T., 1994, Transport modeling in heterogeneous aquifers, 1, Statistical description and numerical generation, Water Resources Research, 30(6), 1803–1817.

Kitanidis, P., 1995, Quasi-linear geostatistical theory for inversing, Water Resources Research, 31(10), 2411-2419.

Klingbeil, R., Kleineidam, S., Asprion, U., Aigner, T., and Teutsch, G., 1999, Relating lithofacies to hydrofacies: Outcrop-based hydrogeological characterization of Quaternary gravel deposits, Sedimentary Geology, 129(3-4), 299-310.

Lunt, I., Bridge, J., and Tye, R., 2004, A quantitative, three-dimensional depositional model of gravelly braided rivers, Sedimentology, 51(3), 377-414.

Malama, B. and Johnson, B., 2010, Analytical modeling of saturated zone head response to evapotranspiration and river-stage fluctuations, Journal of Hydrology, 382, 1-9, doi:10.1016/j.jhydrol.2009.12.010.

Malama, B., Kuhlman, K.L., Barrash, W., Cardiff, M., and Thoma, M., 2011, Modeling slug tests in unconfined aquifers taking into account water table kinematics, wellbore skin and inertial effects, Journal of Hydrology, 208, 113-126, doi:10.1016/j.jhydrol.2011.07.028.

Moret, G.J.M., Knoll, M.D., Barrash, W., and Clement, W.P., 2006, Investigating the stratigraphy of an alluvial aquifer using crosswell seismic traveltime tomography, Geophysics, 71(3), B63-B73, 10.1190/1.2195487.

Morin, R., LeBlanc, D., and Teasdale, W., 1988, A statistical evaluation of formation

disturbance produced by well-casing installation methods, Ground Water, 26, 207-217.

Mwenifumbo, C.J., Barrash, W., and Knoll, M.D., 2009, Capacitive conductivity logging and electrical stratigraphy in a high-resistivity aquifer, Boise Hydrogeophysical Research Site, Geophysics, 74(3), E125-E133, doi:10.1190/1.3106760.

Nelson, G.K., 2007, Deterministic modeling of bromide tracer transport during the Tracer/Time-Lapse Radar Imaging Test at the Boise Hydrogeophysical Research Site, August 2001: MS Thesis, Boise State University, Boise, ID.

Reboulet, E.C. and Barrash, W., 2003, Core, grain-size, and porosity data from the Boise Hydrogeophysical Research Site, Boise, Idaho: BSU CGISS Technical Report, 03-02, Boise State University, Boise, ID, 84 p.

Rehfeldt, K.R., Boggs, J.M., Gelhar, L.W., 1992, Field study of dispersion in a heterogeneous aquifer, 3. Geostatistical analysis of hydraulic conductivity: Water Resources Research, v. 28, no. 12, p. 3309-3324.

Slater, L., Binley, A., Barrash, W., Keery, J., Montrey, J., and Cardiff, M., 2011, An investigation of the ability of induced polarization to resolve aquifer heterogeneity in an unconsolidated sedimentary aquifer (abs.): SAGEEP, April 2011, Charleston, SC.

Straface, S., Chidichimo, F., Rizzo, E., Riva, M., Barrash, W., Revil, A., Cardiff, M., and Guadagnini, A., 2011, Joint inversion of steady-state hydrologic and self-potential data for 3D hydraulic conductivity distribution at the Boise Hydrogeophysical Research Site, Journal of Hydrology, 407(104), 115-128, doi: 10.1016/jhydrol.2011.07.013.

Sudicky, E.A., 1986, A natural gradient experiment on solute transport in a sand aquifer: Spatial variabilityof hydraulic conductivity and its role in the dispersion process: Water Resources Research, v. 22, no. 13, p. 2069-2082.

Wolf, S.H., 1988, Spatial variability of hydraulic conductivity in a sand and gravel aquifer: M.S.C.E. Thesis, Department of Civil Engineering, MIT, Cambridge, MA, 118 p.

Zappa, G., Bersezio, R., Felletti, F., and Giuduci, M., 2006, Modeling heterogeneity of gravel-sand, braided stream, alluvial aquifers at the facies scale, Journal of Hydrology, 325, 134-153.

Zlotnik, V., Zurbuchen, B., Ptak, T., and Teutsch, G., 2000, Support volume and sale effect in hydraulic conductivity: Experimental aspects: in Zhang, D. and Winter, C., eds., Theory, modeling, and field investigation in hydrogeology, A special volume in honor of Shlomo P. Neuman's 60th birthday: Boulder, CO, Geological Society of America Special Paper 348, 215-231.

Table 1. Progression of methods used to investigate distribution and structure in univariate and joint K, porosity (φ), and capacitive conductivity (CC) data, and grain size distribution (GSD) data.

Purpose / Scale of Investigation	Treatments and Statistical Tests	Results	Presentation of Results
Investigation of BHRS slug-K data (modeled with updated wellbore-skin K)	Calculated mean, variance, maximum, minimum	*Similar to other deposits *Low-moderate heterogeneity *Validate with hydraulic tomography	Table 3A; Figure 4
Investigation of K distributions within defined φ/CC units	t tests between φ/CC stratigraphic units	*Lower units different, upper similar *One different K relative magnitude ranking from porosity ranking	Table 3B; Figure 5
Recognition of small-scale bodies or facies based on well profiles of K alone	5-pt moving average filters with log10K and standard deviation log10K	*Semi-quantitative interpretation *Many ~1-2m-thick bodies *Contacts consistent with φ/CC unit boundaries	Figure 6
Recognition of small-scale bodies or facies based on multivariate (K, φ, CC) data	Plots and PCA of transformed (normalized) log10K, std dev log10K, φ, and CC	*Local bodies of several multivariate facies types *Local bodies in adjacent wells at similar elevation intervals *Interpretable PCA eigenvectors	Table 4; Figures 7-9; Table S1
Identity and stratigraphic significance of small-scale multivariate facies	MANOVA between facies, and between facies and "host"	*Seven multivariate facies types with occurrence in ≥ 3 adjacent wells *One type repeats vertically *Facies occur exclusively within φ/CC units with few exceptions	Tables 4-5; Figures 9-10; Table S2
Investigation of parameter (petrophysical?) relations or associations within multivariate facies	Cross-plots of parameter pairs by multivariate facies type	*Petrophysical or correlation relationships are not evident *"Mean" parameter associations are apparent	Table 4; Figure 10
Significance of K variation between multivariate facies, and distribution of K-facies	t tests on log10K between vertically adjacent facies, and between facies and hosts	*Distinctions between K-facies types evident for six of seven multivariate facies; *Spatial distributions are laterally continuous	Tables 4, 6; Figures 6, 9, 11; Table S2
Interpretation of small-scale bodies or facies based on GSD data included in multivariate (K, φ, CC, GSD) analysis	8-way PCA on 5 transformed GSD indicators and transformed K, φ, and CC	*Interpretable PCA eigenvectors *Repeated GSD types between facies *Cobble size and volume fraction, sorting, and matrix grain size are GSD parameters with most apparent influence on K *Parameter influences commonly change as K or φ change from lower to higher magnitudes	Tables 7-8; Figures 12-13; Tables S3-S9 and Figures S1-S6

Table 2. K estimates and measurements from previous studies at the BHRS							
Test type	Test Dates	Number of wells, zones	Stimulation	Analysis	Effects considered	K results	References
2D fully penetrating, pumping	1998-1999	18 Q wells, 3-5 obs wells per test	Q = 25-35 gpm, several >40 gpm	Analytical solution, Barrash et al., 2006	Unconfined, skin at Q and obs wells, anisotropy	Kave= 7.6E-4 m/s, anisotropy: 1-2	Fox, 2006; Barrash et al., 2006
1D multi-level slug tests	2008-2009	18 wells, 518 0.3m zones tested in sedimentary	5cm-30cm (pneumatic) slug height	Analytical solution, Malama et al., 2011	Unconfined, skin, partial penetration, inertial effects	Kave range by porosity/capacitive conductivity unit 4.6E-4 to 4.3E-3 m/s	Cardiff et al., 2011; Barrash and Cardiff, this paper
3D transient hydraulic tomography	2010, 2011	2 Q wells, 3-4 obs wells, 21 to 28 1m zones (2010) 1 Q well, 5 obs wells, 35 1m zones (2011)	Q ~ 5-7 gpm and 8-10 gpm for 15-20 min, from 1-m-long zones	Fwd: MODFLOW, Inverse: Adj. state (Clemo, 2007) and geostatistical (Kitanidis, 1995)	Unconfined, transient, >100,000 distributed parameters	K range= 3.4E-5 to 1.3E-3 m/s Kave = 3.0E-4 m/s	Cardiff et al., 2012; Cardiff et al., in review
2D-3D transient hydraulic tomography	2002	1 Q well, 5 obs wells, 35 1m zones	Q ~ 5 gpm for 15-20 min, from 1-m-long zones	Fwd: MODFLOW, Inverse: PEST (limited analysis of partial data set)	Unconfined, transient, constant K in each of 5 units	Kave range by porosity unit 5.3E-5 to 1.6E-3 m/s	Barrash et al., 2007
2D SS dipole hydraulic tomography	2007	Q-I=10 well pairs, 14 obs wells per test	Q-I ~60-70 gpm for 5 hr, then recovery	Fwd: Potential difference, Inverse: geostatistical (Kitanidis, 1995)	Unconfined, steady-state, distributed	K range = 6.3E-5 to 1.4E-3, Kave = 6.3E-4	Cardiff et al., 2009
3D SS dipole hydraulic tomography, geophysics	2007	Q-I=10 well pairs, 14 obs wells per test	Q-I ~60-70 gpm for 5 hr, then recovery	Joint head-SP with 3D multiple indicator, and K estimated by max. likelihood	Unconfined, steady-state, SP; K distributed in 5 sedimentary units	Kave range by porosity unit 5.6E-5 to 1.3E-3 m/s	Straface et al., 2011
2D transient ET-river-aquifer	2008	1 well	Diurnal ET signal	Analytical solution, Malama and Johnson, 2010	Unconfined, transient, ET, fully penetrating river	K=3.4E-4 m/s	Malama and Johnson, 2010
3D transient conservative tracer test	2001	Inj. well, obs well 20 zones, 5 margin wells 6 zones	"Plug" injection, ~natural gradient, minor Q recovery	MODFLOW, SEAWAT, MT3DMS	Unconfined, transient, density, river leakage, var-iable layering	K homogeneous = 3E-4 m/s K range (≥ 5 layers) = 1E-4 to 1E-3 m/s	Nelson, 2007

Table 3A. Log10K (m/s) population statistics by porosity-electrical conductivity units for 13 central area wells at the BHRS

Units	n	Log10K Mean m/s	Log10K Variance m^2/s^2	Log10K Maximum	Log10K Minimum
All	518	-3.045	0.093	-1.800	-4.192
5	10	-3.008	0.020	-2.749	-3.247
4	143	-3.023	0.084	-2.272	-3.704
3	118	-3.034	0.076	-2.227	-3.561
2B	42	-2.770	0.125	-1.800	-3.261
2A	165	-3.059	0.074	-2.330	-4.192
2 (2B and 2A)	207	-3.001	0.097	-1.800	-4.192
1	40	-3.390	0.050	-3.012	-3.938

Table 3B. Statistical differences at 0.05 level in log10K populations between porosity-electrical conductivity units for 13 central area wells at the BHRS

Unit Pair	n 1	n 2	Total n	t statistic	t value	Accept or Reject H_o
3 and 4	118	143	261	0.327	<1.9719, >1.960	*Accept*
2B and 3	42	118	160	4.410	1.9751	*Reject*
2A and 3	165	118	283	0.755	<1.9719, >1.960	*Accept*
2A and 2B	165	42	207	4.961	1.9719	*Reject*
1 and 2A	40	165	205	8.035	1.9719	*Reject*

Two-tailed test; df = n - 2

Table 4. Multivariate and Univariate K-Facies Occurrence and Characteristics

Multivariate K-Facies	Univariate K-Facies	Bottom Ele (m)	Top Ele (m)	Porosity/CC Unit	Log10K	Std Dev Log10K	Porosity	CC	Wells
H	H	843.6	844.8	4	low	low	very high	very high	C3,C4,C5
G	G	842.9	844.5	4	medium	low	high	high	B1,B2,B3,B5,C1,C2
F	F** of EF type	840.2	842.8	3	high	medium	low	low	A1,B1,B2,B6,C1,C5
E	E** of EF type	838.4	841.4	3	high	high	low	very low	B2,B3,B4,B5,C1,C2
D	D	838.1	841.3	2B	very high	very high	medium	very low	B1,B5,B6,C5,C6
C* of BC type	C* of BC type	836.6	838.4	2A	medium	medium	high	medium	B3,B6,C2,C4,C5
B* of BC type	B* of BC type	834.1	835.9	2A	medium	medium	high	medium	A1,B1,B3,B4, B5,C2,C3,C4
A	A	≤833	834+	1	low	very high	low	medium	All except C5

* Multivariate and univariate K-facies B and C are not distinguishable statistically (Tables 5-6) but are identified separately here because they are not vertically contiguous bodies.

** Univariate K-facies E and F are not distinguishable statistically based on log10K (Table 6) but are identified separately here because they have different multivariate statistics (Table 5) and appear to be vertically superimposed separate bodies.

37

Table 5. MANOVA results comparing multivariate facies and facies vs host sediments at the same elevation range as facies

Multivariate K-Facies Pair	N Facies 1	N Facies 2	Total n	Λ	χ^2 Statistic	χ^2 0.05**	Accept or Reject H_o
B and C	31	21	52	0.880	5.96	7.81	*Accept*
A*** and BC	44	50	94	0.277	116.27	7.81	Reject
BC and BC Host	50	89	139	0.785	32.80	7.81	Reject
BC and D	50	24	74	0.142	137.70	7.81	Reject
D and D Host	24	52	76	0.423	62.34	7.81	Reject
D and E	24	34	58	0.405	49.25	7.81	Reject
E and E Host	34	45	79	0.625	35.54	7.81	Reject
E and F	34	28	62	0.596	30.32	7.81	Reject
F and F Host	28	50	78	0.686	28.11	7.81	Reject
D and EF*	24	62	86	0.409	73.74	7.81	Reject
EF and EF Host *	62	95	157	0.662	63.33	7.81	Reject
EF and G*	62	21	83	0.175	138.73	7.81	Reject
G and G Host	21	38	59	0.531	35.10	7.81	Reject
G and H	21	13	34	0.313	35.41	7.81	Reject
H and H Host	13	25	38	0.282	43.63	7.81	Reject

* E and F, and E and E Host have similar log10K populations based on t tests (see Table 7).
** χ^2 for MANOVA evaluated for all pairings at df=(g-1)p and α=0.05 where g = 2 groups and p = 3 parameters (Johnson and Wichern, 1998).
*** A is not compared to Host because this facies extends across the study area.

Table 6. Statistical differences at 0.05 level in log10K populations between multivariate K-facies

K Facies Pair	n Facies 1	n Facies 2	Total n	t Statistic	t 0.05	Accept or Reject H_o
B and C	31	21	52	1.6928	2.0086	*Accept*
B and B Host	31	36	67	3.2982	1.9971	Reject
C and C Host	21	53	74	5.3388	1.9935	Reject
A and BC	44	50	94	4.1836	1.9861	Reject
BC and BC Host	50	89	139	6.4147	1.9774	Reject
BC and D	50	24	74	13.0254	1.9935	Reject
D and D Host	24	52	76	8.8689	1.9925	Reject
E and E Host	34	45	79	1.0890	1.9913	*Accept*
F and F Host	28	50	78	3.0283	1.9917	Reject
E and F	34	28	62	0.1752	2.0003	*Accept*
D and EF	24	62	86	8.7006	1.9886	Reject
EF and EF Host	62	95	157	2.9698	1.9754	Reject
EF and G	62	21	83	6.4566	1.9897	Reject
G and G Host	21	38	59	2.6371	2.0025	Reject
G and H	21	13	34	7.4227	2.0369	Reject
H and H Host	13	25	38	9.6833	2.0281	Reject

Two-tailed test; df = n - 2

Table 7. Occurrence, composition, and variance percent of 8-way principal components with major K loading

K-facies	All	All	H	G	G	G	A	BC	D	A	BC	A	H	EF	EF	H
Treatment	*-1	*-1		*-1	*-1	*-1	*-1	*-1	*-1		*-1				*-1	*-1
PC (Eigenvector)	5	6	7	7	6	5	6	7	7	5	5	7	5	5	6	6
Variance %	11.5%	13.2%	17.0%	20.5%	14.1%	6.0%	13.9%	20.1%	21.2%	10.1%	10.7%	19.1%	5.1%	9.9%	18.4%	12.6%
K	0.727	0.593	0.415	0.330	0.554	0.591	0.518	0.611	0.687	0.426	0.487	0.543	0.316	0.825	0.452	0.819
m porosity	-0.349	0.194	0.766	-0.266	-0.108	-0.399	-0.161	-0.093	0.447	0.065	0.435	0.327	0.095	0.108	-0.267	-0.317
CC	-0.093	-0.279	0.194	-0.614	-0.358	0.669	0.194	0.220	-0.423	-0.495	0.339	0.629	0.433	0.246	-0.342	-0.426
all 60	-0.114	-0.104	0.136	-0.085	0.035	0.001	0.063	0.046	-0.277	-0.205	0.052	0.017	-0.004	-0.131	0.020	0.084
all 60/10	0.244	-0.359	0.047	0.161	-0.163	0.000	0.477	0.265	-0.238	-0.441	-0.415	-0.182	-0.013	-0.053	0.224	0.015
m 10	-0.394	0.497	0.382	-0.370	0.352	-0.176	-0.571	-0.201	-0.033	-0.244	0.482	0.347	-0.695	-0.172	0.156	0.009
m 60/10	-0.206	0.337	0.127	0.464	-0.628	0.108	-0.128	-0.640	0.079	0.510	0.139	0.164	0.266	0.425	-0.628	-0.194
% cobbles	-0.268	0.182	0.142	-0.240	-0.083	0.024	-0.307	-0.217	-0.094	-0.115	0.177	0.148	-0.387	-0.131	-0.371	-0.037

m porosity is sample porosity assigned to matrix volume

CC is capacitive conductivity

all 60 is the d60 grain size of the whole sample (i.e., cobble size indicator)

all 60/10 is d60 divided by d10 for the whole sample (i.e, sorting indicator)

m 10 is the d10 grain size of matrix grains (<9.525 mm)

m 60/10 is d60 divided by d10 for the matrix fraction (i.e, sorting indicator)

% cobbles is the solid volume fraction larger than 9.525 mm (i.e., framework proportion indicator)

Key to color scales for parameter loadings on PCs with major K loading: positive (greens) and negative (browns)

color scale	>0.5	.3 to .5	.1 to .3	0 to .1
color scale	<-0.5	-.3 to -.5	-.1 to -.3	0 to -.1
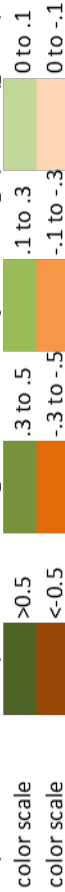
Descriptions of PCs with major K loading that are repeated in different K-facies:

repeated PC (eigenvector) type: high K-low matrix porosity with >CC, <d10m, good matrix sorting, and <cobbles

repeated PC (eigenvector) type: high K-high matrix porosity with <CC, small well-sorted cobbles, <d10m and average to poor matrix sorting

repeated PC (eigenvector) type: high K-high matrix porosity with >CC, >d10m, poor matrix sorting, and more than average cobble %

repeated PC (eigenvector) type: high K-high matrix porosity with >CC, <d10m, poor matrix sorting, and low % cobbles

repeated PC (eigenvector) type: high K-low matrix porosity with <CC, good matrix sorting, and average to low %cobbles

	Table 8. PC parameter comparisons in order of increasing log10K and increasing porosity				
A	parameter comparisons in order of increasing log10K				
			correlation coefficient	significance test	comparison at 0.05
	low to mid K	n			
	m-porosity v %cobbles (H5-G6, see Figure 13A)	9	**0.803**	**3.559**	**2.365**
	m-porosity v 60/10m (H5-A5, see Figure 13B)	4	-0.837	-2.162	4.303
	m-porosity v 60/10m (EF6-G6, see Figure 13B)	5	0.848	2.776	3.182
	m-porosity v d10m (G7-A7, see Figure 13B)	7	0.733	2.413	2.571
	60/10-all v %cobbles (H5-A7, see Figure 13C-A)	8	-0.600	-1.836	2.447
	m-porosity v CC (H5-G6, see Figure 13C)	9	0.609	2.030	2.365
	m-porosity v CC (G5-EF5, see Figure 13C)	5	-0.463	-0.905	3.182
			correlation coefficient	significance test	comparison at 0.05
B	upper K	n			
	m-porosity v d60-all (BC7-EF5, see Figure 13A)	4	**-0.978**	**-6.565**	**4.303**
	m-porosity v %cobbles (G5-EF5, see Figure 13A)	5	-0.454	-0.881	3.182
	m-porosity v 60/10m (BC7-EF5, see Figure 13B)	4	0.490	0.796	4.303
	60/10-all v d60-all (BC7-EF5, Figure 13C-A)	4	0.820	2.028	4.303
	60/10-all v %cobbles (BC7-EF5, Figure 13C-A)	4	-0.640	-1.177	4.303
C	parameter comparisons in order of increasing porosity				
			correlation coefficient	significance test	comparison at 0.05
	low to mid porosity	n			
	log10K v d60-all (G5-A5, see Figure 13D)	8	0.665	2.180	2.447
	log10K v %cobbles (G5-H5, see Figure 13D)	9	0.635	2.177	2.365
	d10-m v 60/10m (G5-BC7, see Figure 13E)	7	-0.620	-1.767	2.571
	CC v 60/10all (H6-A5, see Figure 13F)	7	0.637	1.849	2.571
			correlation coefficient	significance test	comparison at 0.05
D	upper porosity	n			
	log10K v 60/10m (EF5-H7, see Figure 13E)	5	0.689	1.647	3.182
	CC v log10K (H5-H7, see Figure 13F)	6	-0.415	-0.912	2.776
	log10K v d60-all (H5-H7, see Figure 13D)	6	-0.704	-1.982	2.776
	log10K v %cobbles (EF5-H7, see Figure 13D)	5	**-0.928**	**-4.311**	**3.182**
	log10K v d10m (EF5-H7, see Figure 13E)	5	**-0.946**	**-5.048**	**3.182**

Figure 1A

1. Example of coarse fluvial deposits in the Boise area that are similar to those at the BHRS: (a)
quarry exposure approximately 10 m high showing layering, and lenses and structures within
layers, and (b) roadcut showing details of lenses and patches within a layer.

Figure 1B

1. Example of coarse fluvial deposits in the Boise area that are similar to those at the BHRS: (a) quarry exposure approximately 10 m high showing layering, and lenses and structures within layers, and (b) roadcut showing details of lenses and patches within a layer.
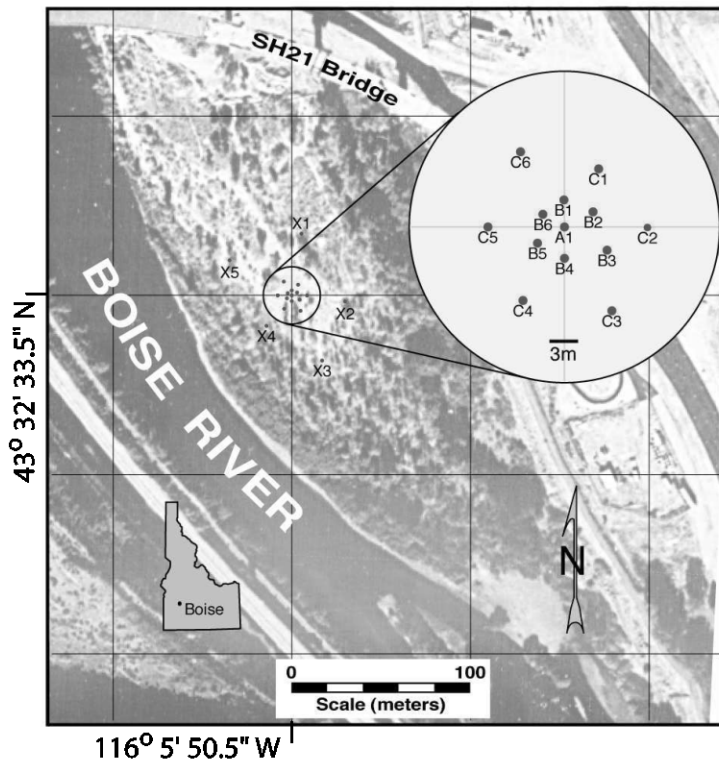
Figure 2. Photomap of the BHRS; inset map shows details of central wellfield.
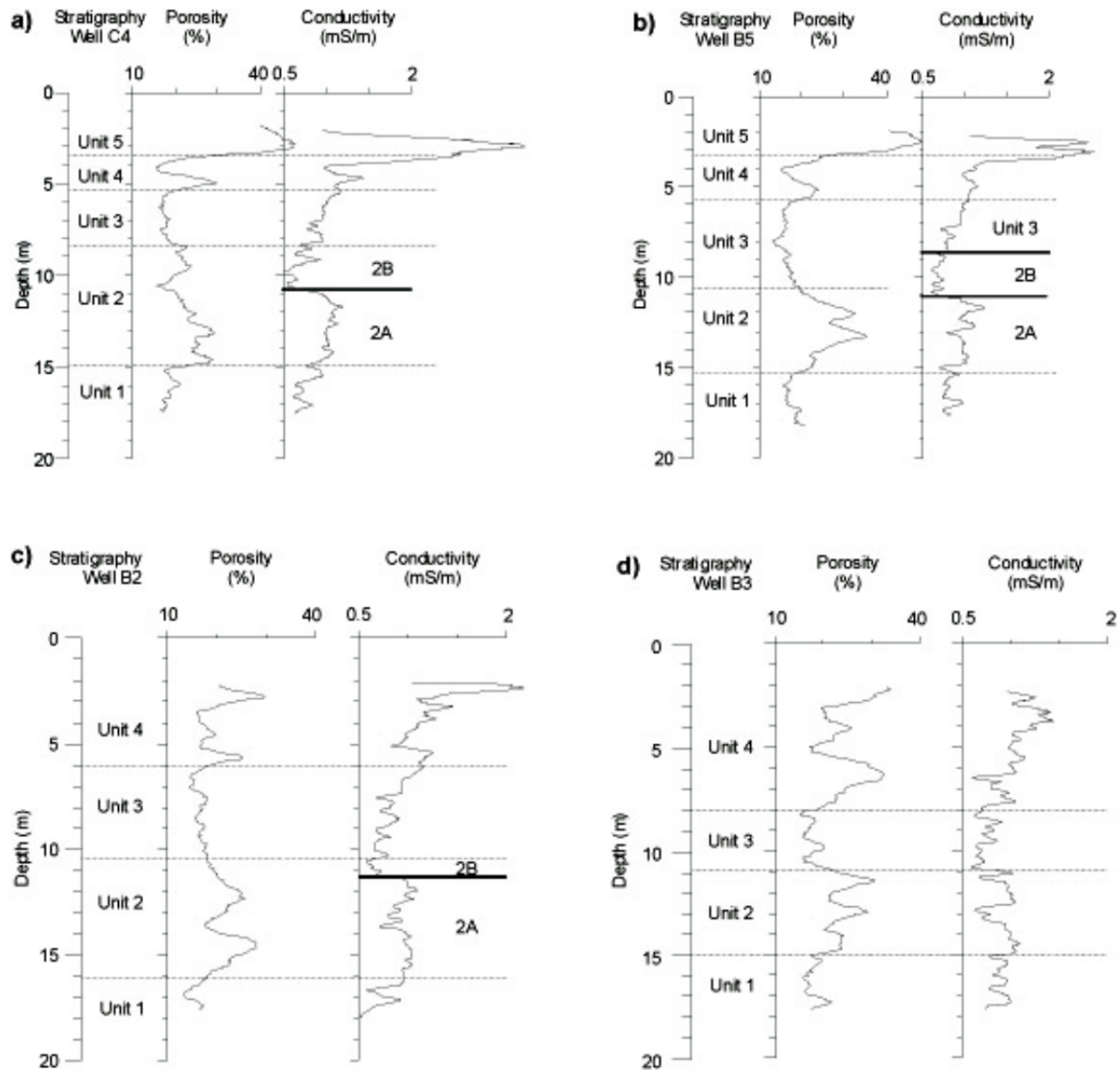
Figure 3. Porosity and capacitive conductivity stratigraphy in four example wells showing general similarity of relative and average porosity and capacitive conductivity magnitudes for units in general (with the exception of Unit 2B), but also showing less similarity between parameters in detail within the units: (a) C4; (b) B5; (c) B2; (d) B3. After Mwenifumbo et al. [2009].
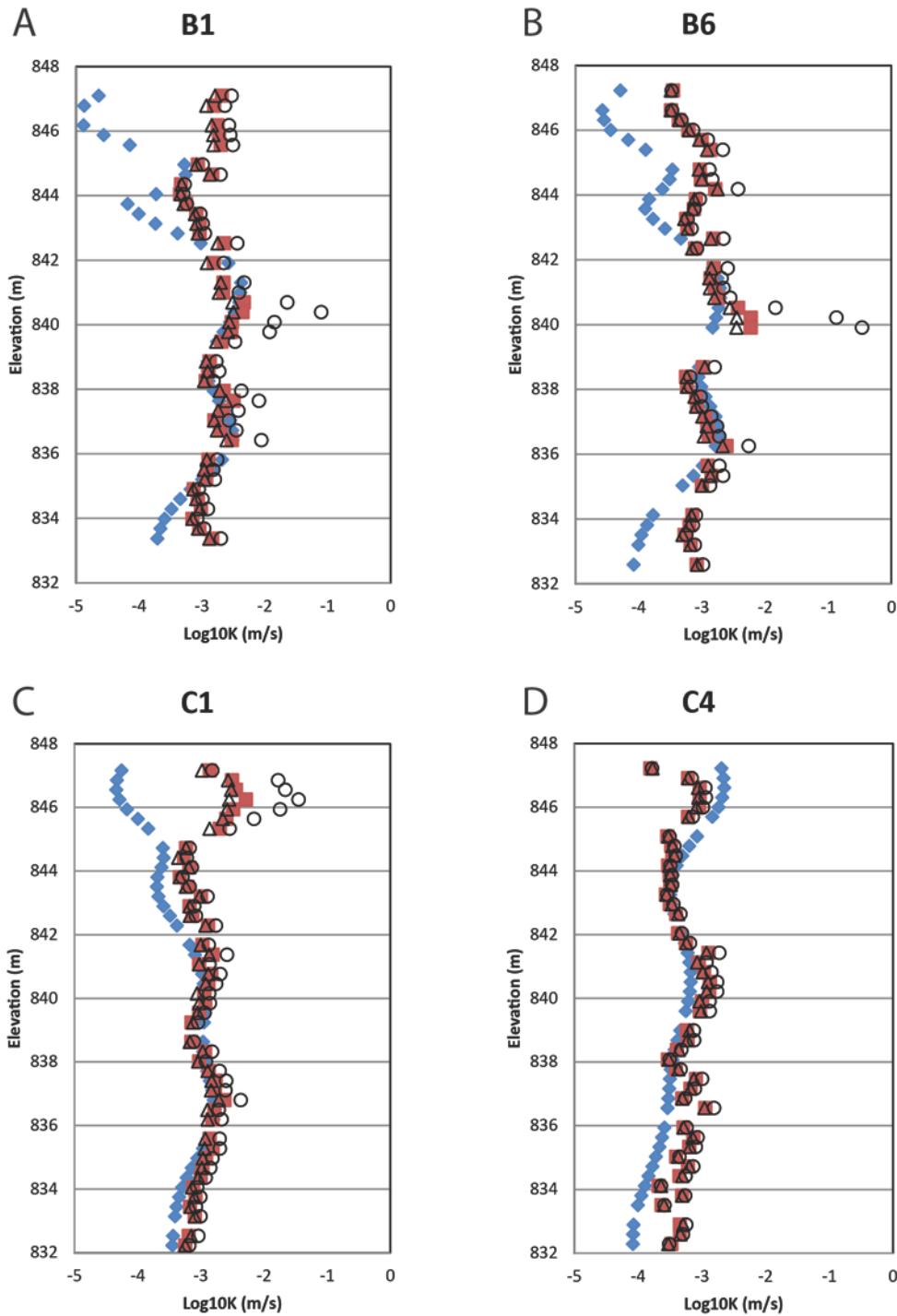
Figure 4. Log10K profile comparisons at four wells between 3D transient hydraulic tomography (blue diamonds) and slug tests analyzed without wellbore skin (triangles), with skin K of 2E-5 m/s (circles), and with skin K of 5E-4 (skin value used for data set evaluated in this paper, red squares). Deviations from matches are greatest at tops and bottoms of profiles where observation coverage was limited or absent during hydraulic tomography testing (Cardiff et al., in review).
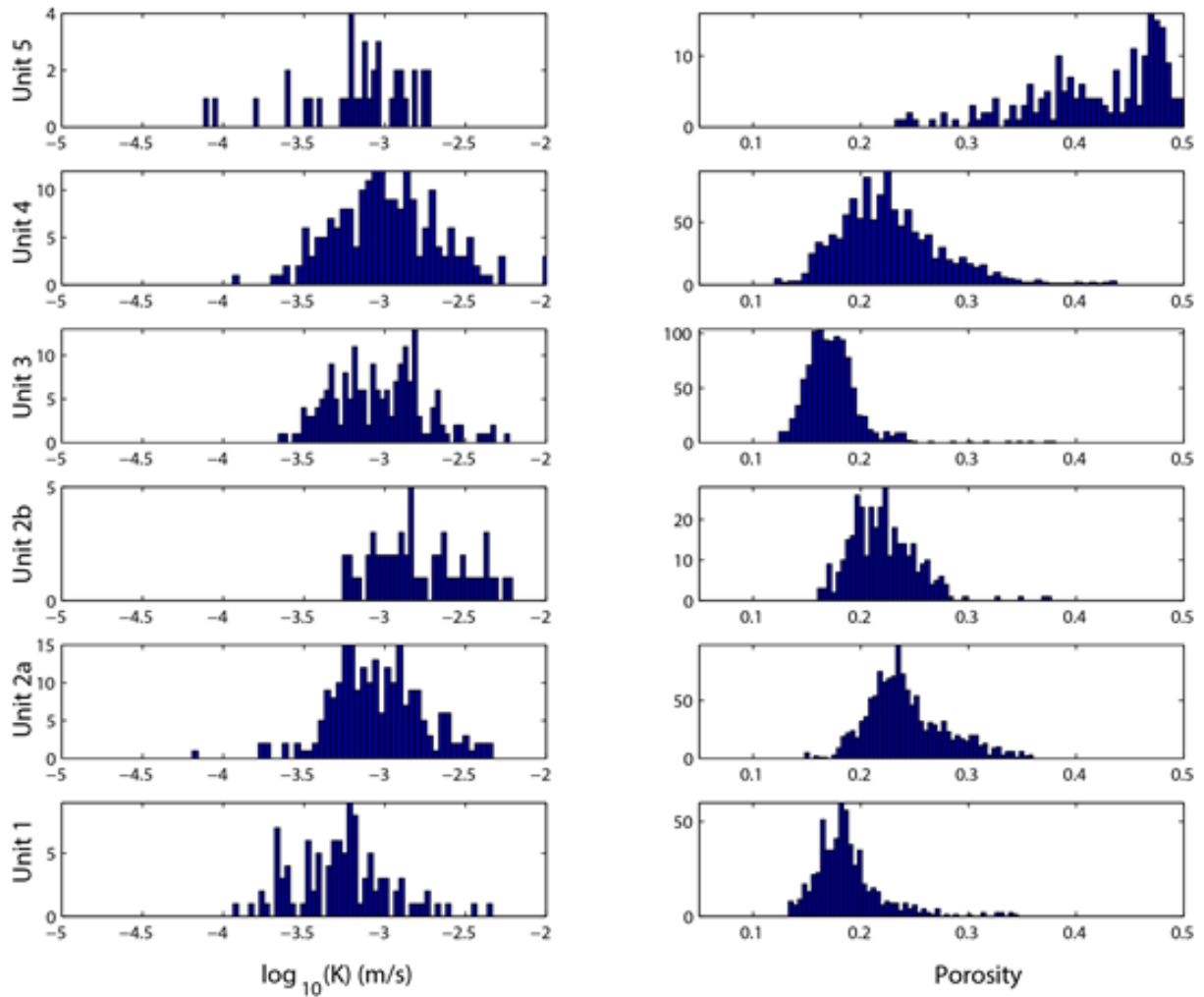
Figure 5. Histogram comparisons for log10K vs porosity show population clustering by porosity and capacitive conductivity stratigraphic units, but the relative magnitudes of log10K vs porosity populations differ between several units.
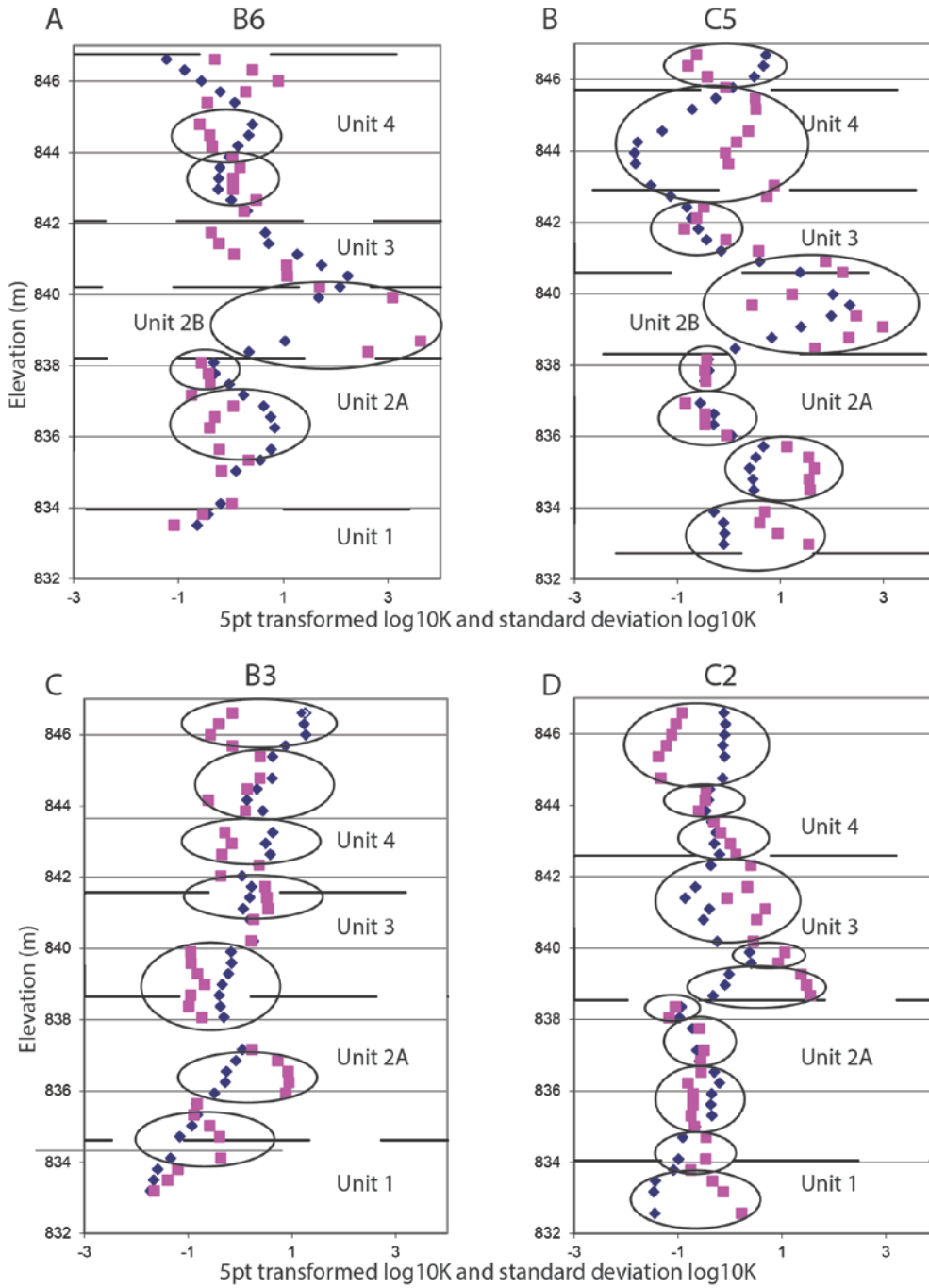
Figure 6. Profiles of 5-pt moving averages of log10K (blue diamonds) and standard deviation log10K (pink squares) transformed to zero mean and unit variance. Locally coherent bodies are outlined by ovals. Porosity and capacitive conductivity unit boundaries are included for perspective.
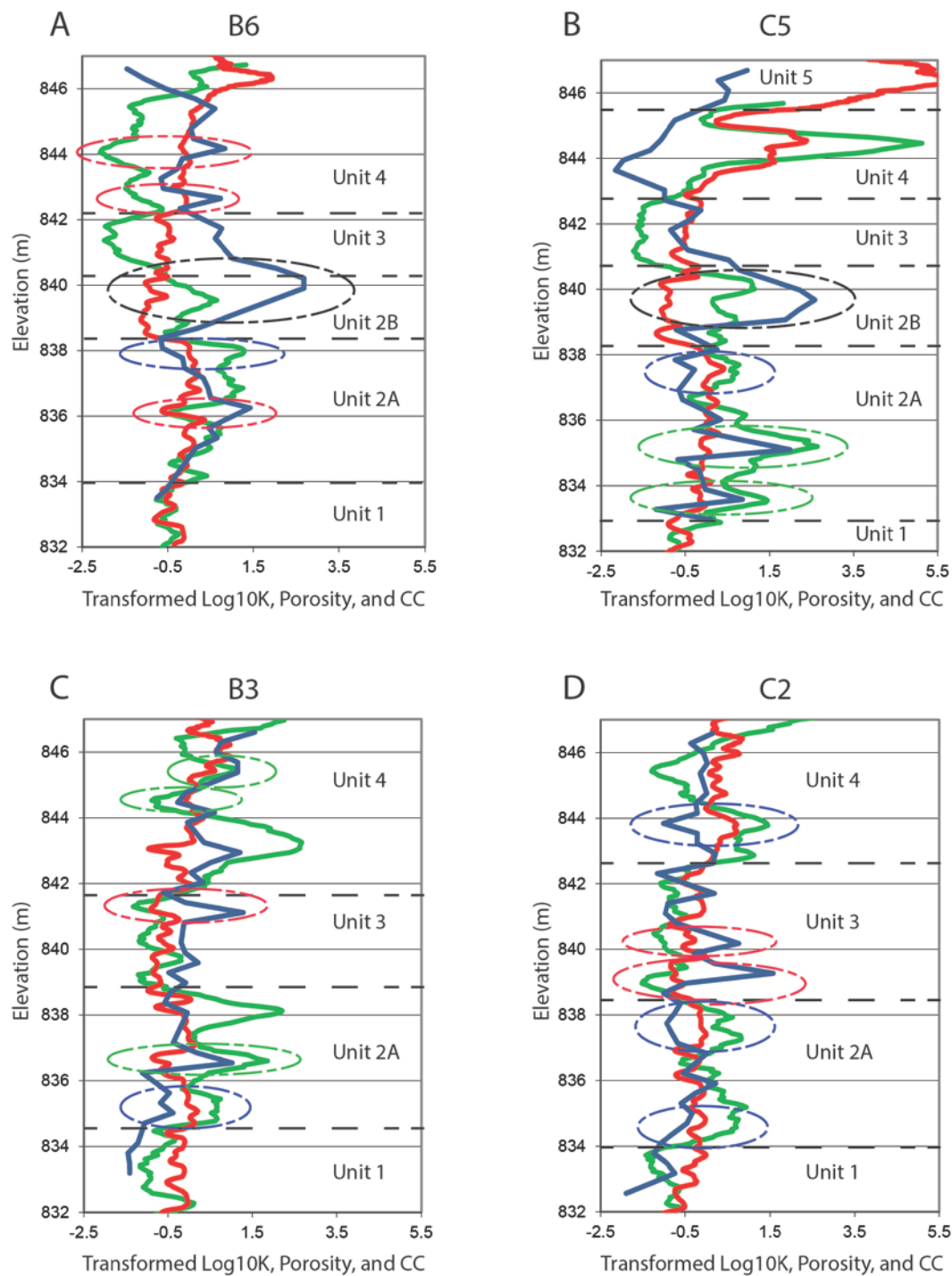
Figure 7. Profiles at four wells of transformed log10K (blue lines), porosity (green lines), and capacitive conductivity (CC, red lines), with types of local facies or lenses identified with dashed oval outlines in the example wells, including: (1) very high K, very low CC, moderate porosity (black oval); (2) high K, high porosity, moderate CC or low K, low porosity, moderate CC (green oval); (3) high K, low porosity, moderate CC (red oval); (4) low K, high porosity, moderate CC (blue oval).

49
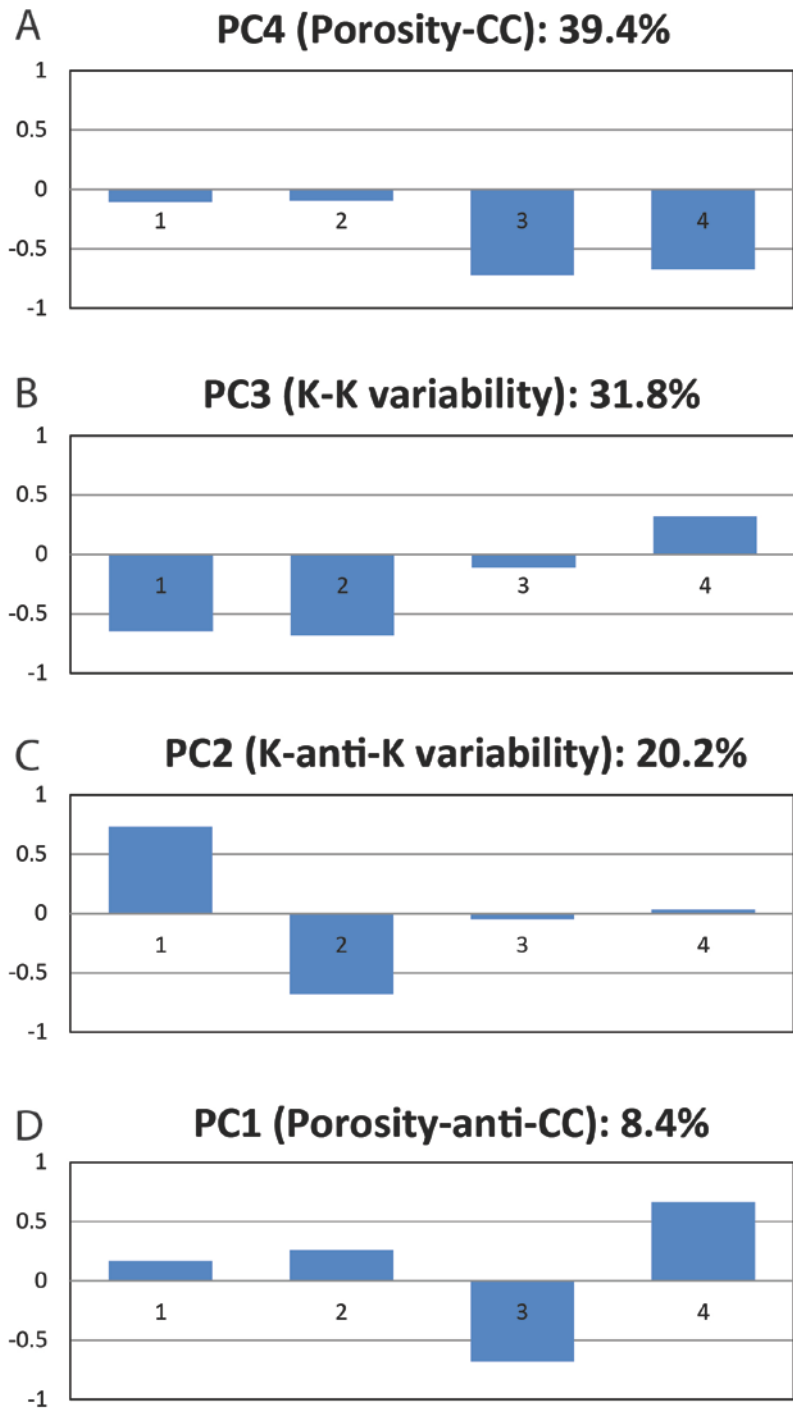
Figure 8. Principal components (PCs are eigenvectors or multivariate orthogonal axes) of 4-way analysis where vector loadings are 1=log10K, 2=standard deviation log10K, 3=porosity, and 4=capacitive conductivity. A. PC4 is dominated by porosity and capacitive conductivity, and explains 39.4% of system variance; B. PC3 is dominated by log10K and standard deviation log10K, and explains 31.8% of the variance; C. and D. PCs 2 and 1 explain remaining variance with respective parameters in opposition.
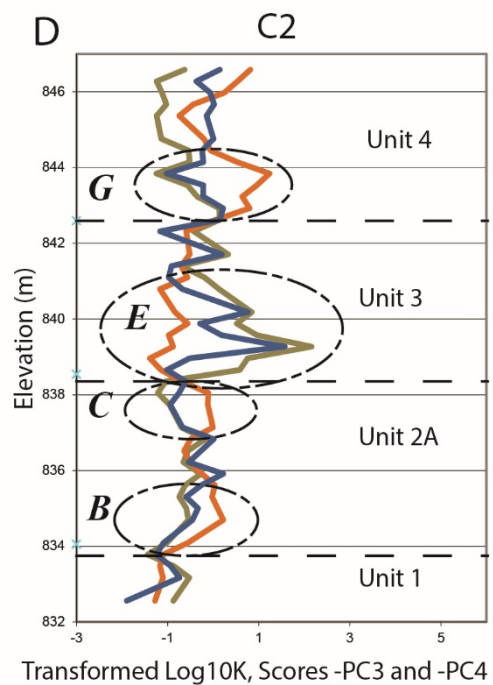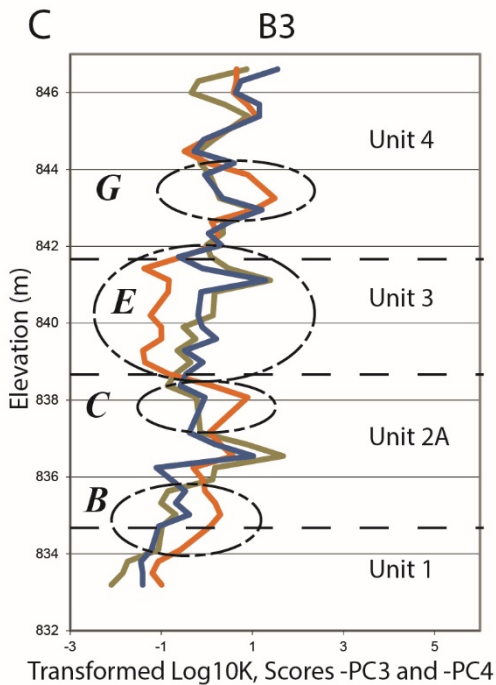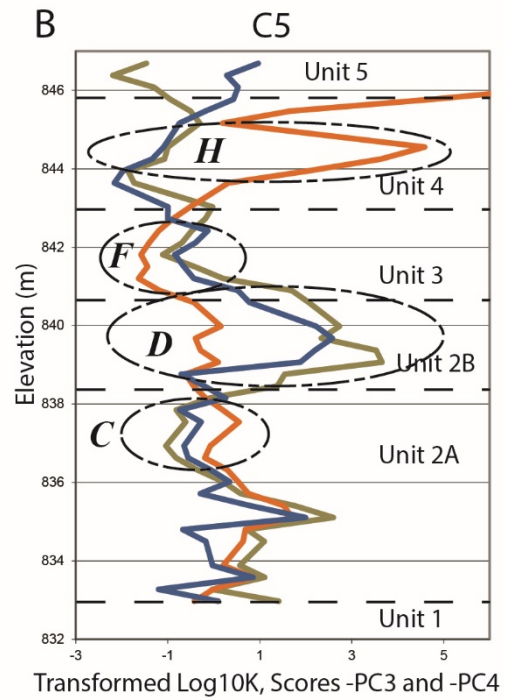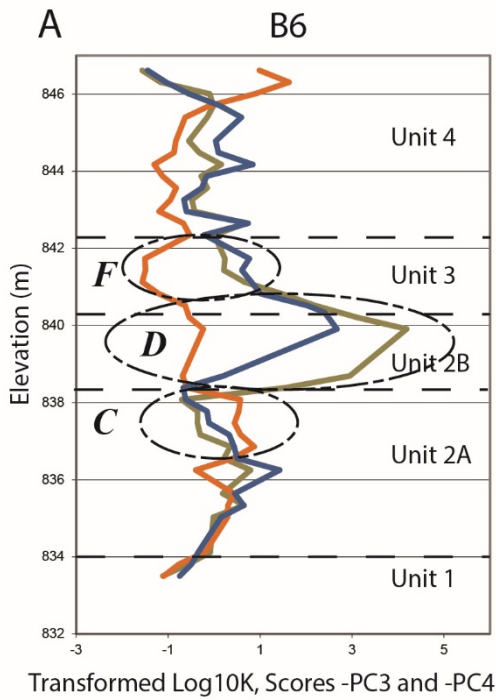
Figure 9. Profiles at four wells of transformed log10K (blue lines) and scores of -PC4 (i.e., porosity and CC; orange lines) and -PC3 (i.e., K and K variability; gray lines). Local coherent bodies evident in adjacent wells are outlined in dashed ovals. PC4 and PC3 are multiplied by (-1) to give all three profiles the same polarity to make log expressions more intuitive in relation to each other.   Bold letters identify repeated types of multivariate K-facies.

51
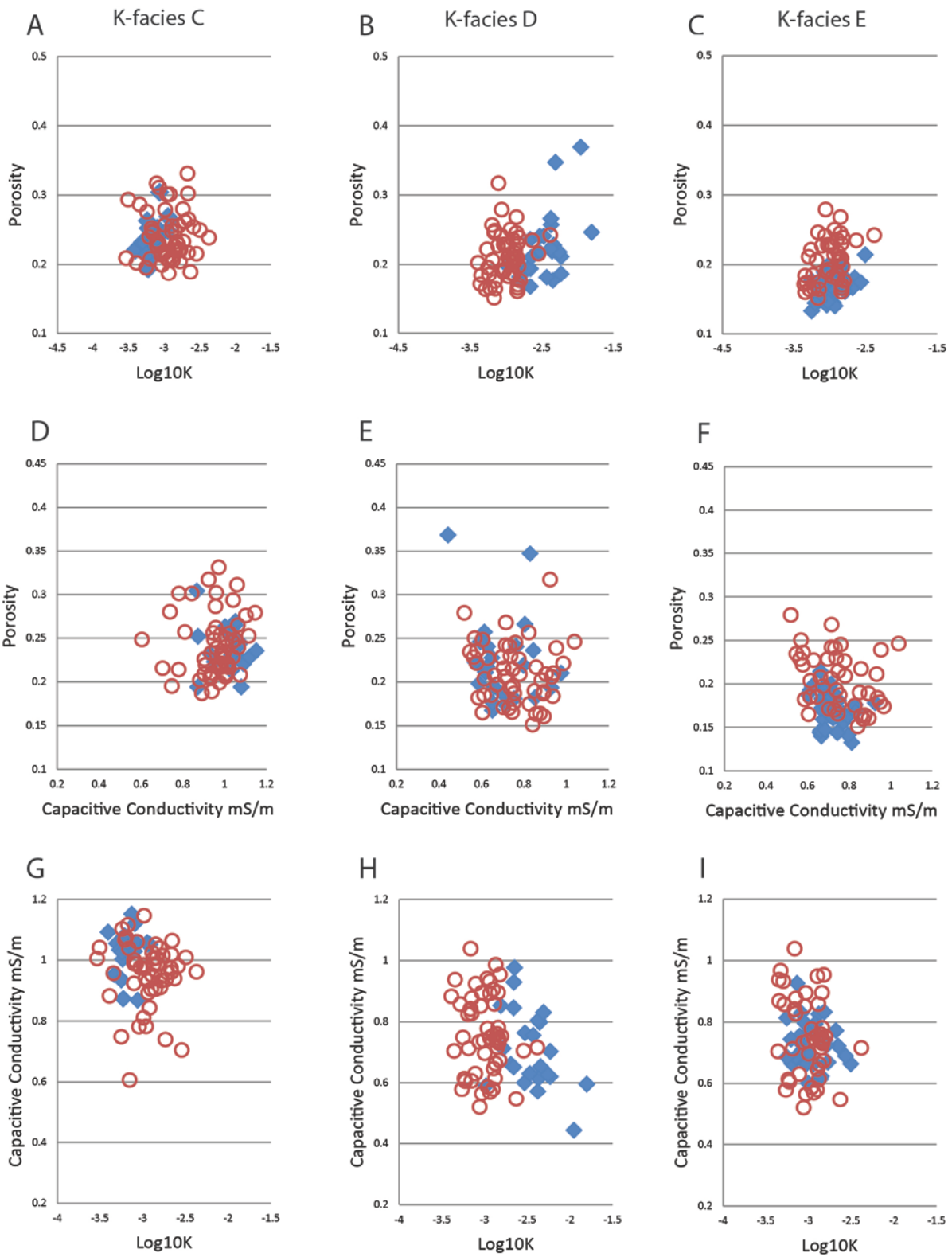
Figure 10. Example crossplots by parameter pairs (rows) showing parameter associations rather than relationships for K-facies C, D, and E (columns). Blue solid symbols for K-facies, red open symbols for Host material at same elevation range as K-facies.
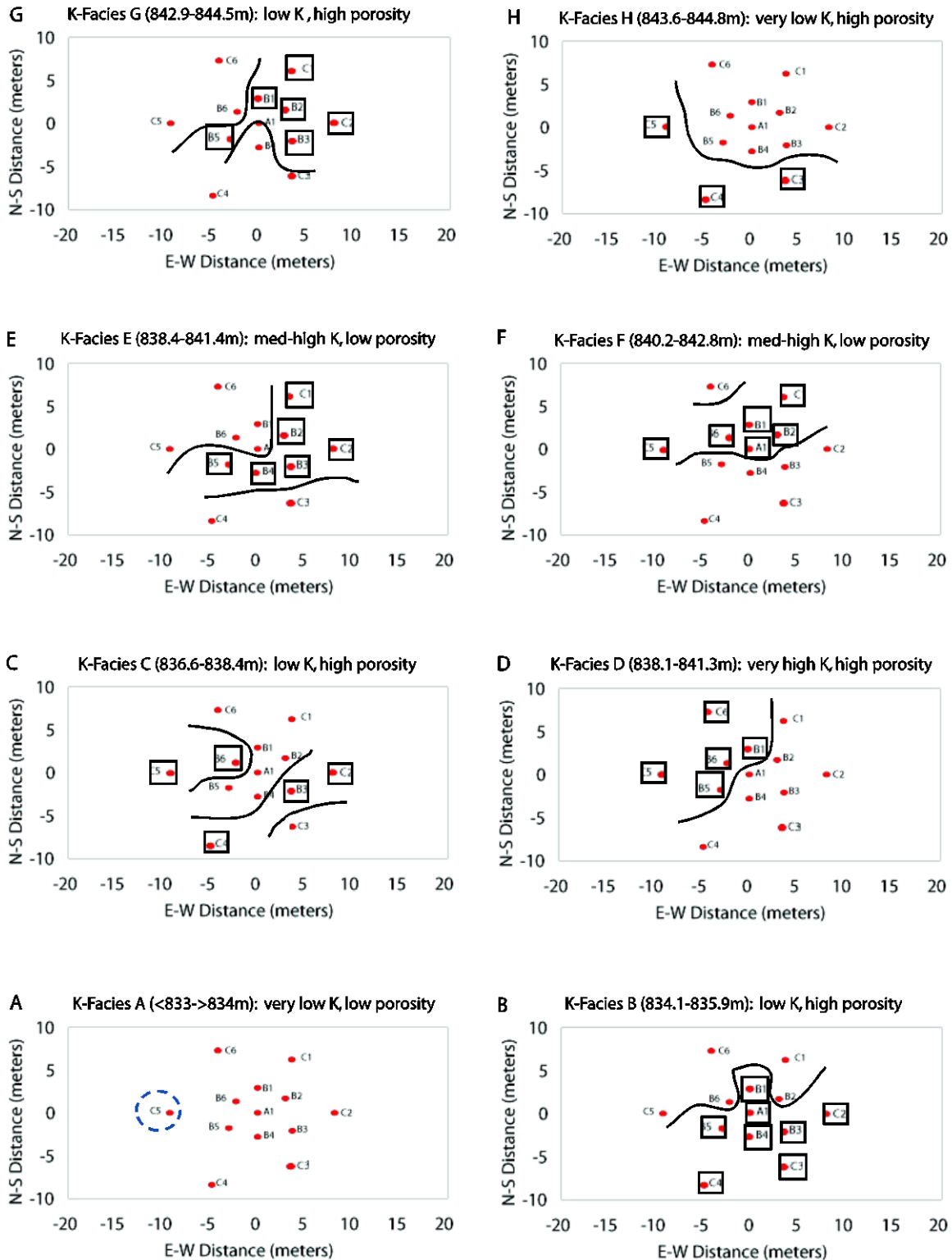
Figure 11. Interpreted areal distribution of "K facies" (see Table 5) in the central area of the BHRS. Wells with facies present are outlined with boxes; circled well in Facies A indicates facies absent there: (a) Facies A ; (b) Facies B ; (c) Facies C ; (d) Facies D ; (e) Facies E ; (f) Facies F; (g) Facies G: (h) Facies H.
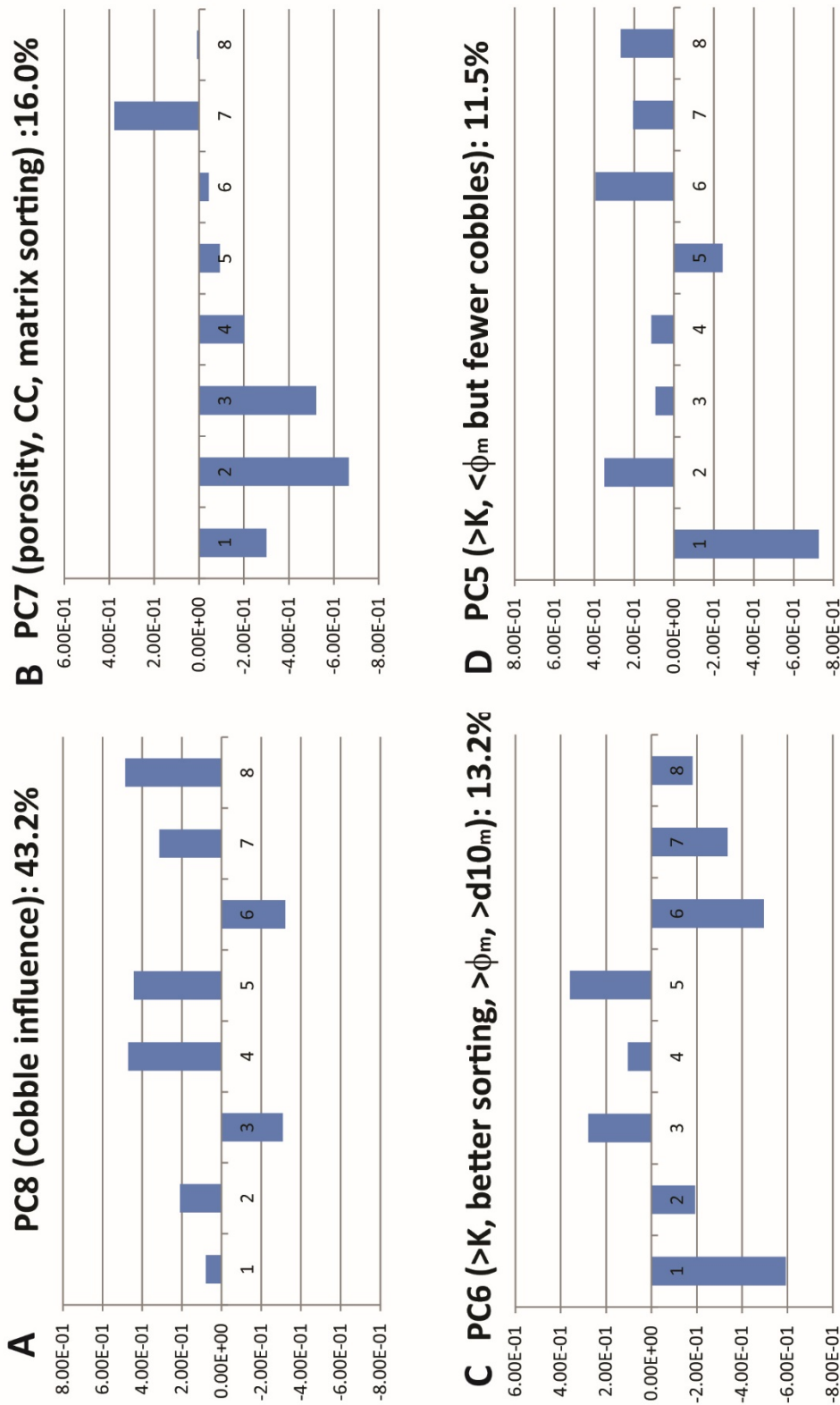
Figure 12. Four eigenvectors explain ~84% of system variance for 8-way PCA that includes grain-size and matrix vs framework parameters. Eight parameters are: 1=log10K (m/s); 2=porosity assigned to matrix; 3=CC or capacitive conductivity (mS/m); 4=d60 of the full sample GSD; 5=d60/d10 of the full sample GSD; 6=d10 of the full sample GSD; 7=d60/d10 of the matrix fraction; 8=volume fraction of grains >9.525mm. A. PC8 indicates much of the system variance is associated with cobble size and volume proportion, overall and relative to matrix. B. PC7 indicates that CC is strongly related to ϕ_m and matrix sorting quality (i.e. lower d60/d10 is better sorting). C. and D. PCs 6 and 5 indicate that K is associated (respectively) with opposite-polarity combinations of matrix porosity, sorting, d10m, and cobble fraction.
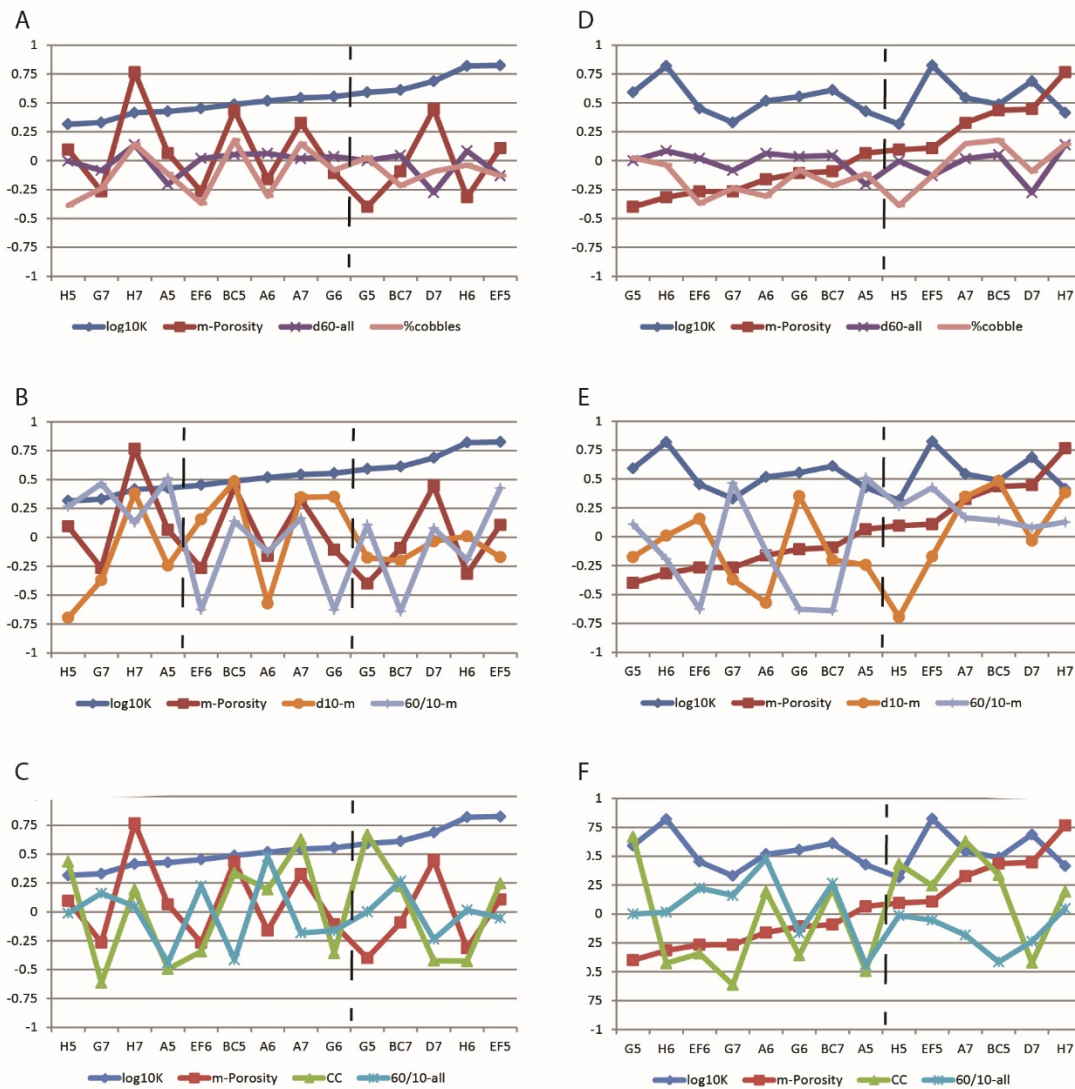
Figure 13. Comparison plots of parameter loadings from 8-way PCA for PCs with significant log10K influence in K-facies, presented in ascending log10K order (A-C) and ascending matrix-ϕ order (D-F) to show joint behavior (also see Table 8). Dashed lines at divisions in individual or collective behavior. A. Cobble size (d60-all) and %cobbles are consistently near to below average; ϕ is highly variable without a trend but mostly varies with %cobbles for low to mid K, and opposite %cobbles for higher K. B. Matrix grain size indicators: poorer sorting (ie >60/10-m) at lower K; smaller to average d10-m at higher K; mostly sorting quality for low and mid K in opposition to d10-m and similar to ϕ; for upper-mid K, sorting quality in opposition with ϕ. C. ϕ mostly follows full sample sorting (ie >ϕ with <60/10-all and vice versa); CC mostly tracks ϕ for lower K but mostly opposite ϕ for higher K. No trend for CC or 60/10-all with K. D. Cobble size and K mostly track for low to mid ϕ then, with %cobbles, are in opposition for higher K. No trends with porosity. E. Matrix sorting mostly tracks with d10-m (ie >60/10m with <d10-m and vice versa) for lower half of ϕ; K tracks with d10-m for upper-mid K, then mostly opposite for upper K; matrix sorting is poor for upper-mid K then average for higher ϕ. F. CC tracks opposite sample sorting quality for low-mid ϕ; CC (relatively high) may be roughly tracking opposite sorting quality for mid-upper ϕ.

55

Supporting Information: Tables S1A-S1C with Statistcs Supporting 4-way PCA

Table S1A. Variance-Covariance Matrix

	log10K	stdevK	porosity	cap con
log10K	1	0.193	0.147	-0.094
stdevK	0.193	1	0.174	-0.134
porosity	0.147	0.174	1	0.573
cap con	-0.094	-0.134	0.573	1

Table S1B. Eigenvectors

	Eigenvector 1	Eigenvector 2	Eigenvector 3	Eigenvector 4
log10K	0.169	0.735	-0.648	-0.107
stdevK	0.263	-0.676	-0.682	-0.097
porosity	-0.680	-0.048	-0.112	-0.723
cap con	0.664	0.032	0.320	-0.675

Table S1C. Eigenvalues

Eigenvector 1	Eigenvector 2	Eigenvector 3	Eigenvector 4
0.337	0	0	0
0	0.809	0	0
0	0	1.275	0
0	0	0	1.580

Supporting Information: Tables S2A-S2C with K-facies population statistics

Table S2A. K-facies log10K population characteristics

Facies	n	Mean m/s	Variance m^2/s^2	Maximum m/s	Minimum m/s
H	14	-3.477	0.0115	-3.272	-3.704
G	21	-3.198	0.0190	-2.938	-3.499
EF	62	-2.958	0.0297	-2.502	-3.303
F	28	-2.962	0.0251	-2.646	-3.303
E	34	-2.954	0.0343	-2.502	-3.253
D	24	-2.447	0.0713	-1.800	-2.983
BC	50	-3.210	0.0232	-2.912	-3.721
C	21	-3.169	0.0174	-2.912	-3.402
B	29	-3.240	0.0260	-2.929	-3.721
A	44	-3.389	0.0652	-3.012	-4.192
HOST	303	-3.002	0.0696	-2.272	-3.762

Table S2B. K-facies porosity population characteristics

Facies	n	Mean	Variance	Maximum	Minimum
H	14	0.257	0.00520	0.409	0.173
G	21	0.226	0.00154	0.326	0.164
EF	62	0.167	0.00052	0.218	0.128
F	28	0.162	0.00068	0.218	0.128
E	34	0.170	0.00037	0.214	0.132
D	24	0.224	0.00244	0.369	0.168
BC	50	0.240	0.00058	0.304	0.194
C	21	0.237	0.00066	0.304	0.194
B	29	0.242	0.00053	0.303	0.194
A	44	0.175	0.00034	0.224	0.133
HOST	303	0.224	0.00303	0.484	0.123

Table S2C. K-Facies capacitive conductivity population characteristics

Facies	n	Mean mS/m	Variance mS^2/m^2	Maximum mS/m	Minimum mS/m
H	14	1.322	0.0673	1.950	1.052
G	21	1.115	0.00625	1.284	0.968
EF	62	0.771	0.00780	0.972	0.601
F	28	0.831	0.00458	0.972	0.718
E	34	0.722	0.00515	0.926	0.601
D	24	0.703	0.0159	0.976	0.443
BC	50	0.998	0.00507	1.151	0.768
C	21	1.017	0.00649	1.151	0.868
B	29	0.983	0.00374	1.074	0.768
A	44	0.857	0.00914	0.992	0.665
HOST	303	1.042	0.143	3.400	0.520

Table S3A. Variance-Covariance Matrix

	K (skin 5E-4)	m porosity	CC	all 60	all 60/10	m 10	m 60/10	% cobbles
K (skin 5E-4)	1	0.178	-0.0828	0.0780	0.0944	-0.0203	0.0393	0.0713
m porosity	0.178	1	0.128	0.414	0.200	-0.0918	0.0736	0.418
CC	-0.0828	0.128	1	-0.335	-0.335	0.211	-0.446	-0.551
all 60	0.0780	0.414	-0.335	1	0.786	-0.390	0.311	0.804
all 60/10	0.0944	0.2005	-0.335	0.786	1	-0.627	0.227	0.601
m 10	-0.0203	-0.0918	0.211	-0.390	-0.627	1	-0.271	-0.326
m 60/10	0.0393	0.0736	-0.446	0.311	0.227	-0.271	1	0.577
% cobbles	0.0713	0.418	-0.551	0.804	0.601	-0.326	0.577	1

K (skin 5E-4) is log10K calculated from slug tests with a wellbore skin value of 5E-4m/s

m porosity is sample porosity assigned to matrix volume

CC is capacitive conductivity

all 60 is the d60 grain size of the whole sample (i.e., cobble size indicator)

all 60/10 is d60 divided by d10 for the whole sample (i.e, sorting indicator)

m 10 is the d10 grain size of matrix grains (<9.525 mm)

m 60/10 is d60 divided by d10 for the matrix fraction (i.e, sorting indicator)

% cobbles is the solid volume fraction larger than 9.525 mm (i.e., framework proportion indicator)

Table S3B. Eigenvectors

	Eigenvector 1	Eigenvector 2	Eigenvector 3	Eigenvector 4	Eigenvector 5	Eigenvector 6	Eigenvector 7	Eigenvector 8
K (skin 5E-4)	0.0106	-0.0850	-0.125	-0.0289	-0.727	-0.593	-0.300	0.0793
m porosity	-0.0655	0.281	0.474	-0.212	0.349	-0.194	-0.667	0.209
CC	0.182	-0.174	-0.589	-0.369	0.0931	0.279	-0.521	-0.309
all 60	-0.664	-0.254	-0.331	0.316	0.114	0.104	-0.200	0.471
all 60/10	0.332	0.631	-0.234	0.210	-0.244	0.359	-0.0928	0.442
m 10	0.0789	0.309	-0.355	0.514	0.394	-0.497	-0.0432	-0.322
m 60/10	-0.134	0.258	-0.348	-0.630	0.206	-0.337	0.378	0.313
% cobbles	0.623	-0.509	-0.0346	0.110	0.268	-0.182	0.00985	0.485

Table S3C. Eigenvalues

	1	2	3	4	5	6	7	8
1	0.0933							
2		0.154						
3			0.390					
4				0.654				
5					0.918			
6						1.053		
7							1.279	
8								3.458

Table S4A. Variance-Covariance Matrix

	K (skin 5E-4)	m porosity	CC	all 60	all 60/10	m 10	m 60/10	% cobbles
K (skin 5E-4)	1	0.045	0.431	-0.177	-0.112	0.0430	0.0470	-0.256
m porosity	0.045	1	0.043	0.713	0.286	-0.177	0.615	0.828
CC	0.431	0.043	1	-0.126	-0.106	0.320	-0.185	-0.0767
all 60	-0.177	0.713	-0.126	1	0.699	-0.420	0.605	0.841
all 60/10	-0.112	0.286	-0.106	0.699	1	-0.495	0.250	0.374
m 10	0.0430	-0.177	0.320	-0.420	-0.495	1	-0.246	-0.171
m 60/10	0.0470	0.615	-0.185	0.605	0.250	-0.246	1	0.657
% cobbles	-0.256	0.828	-0.077	0.841	0.374	-0.171	0.657	1

K (skin 5E-4) is log10K calculated from slug tests with a wellbore skin value of 5E-4m/s

m porosity is sample porosity assigned to matrix volume

CC is capacitive conductivity

all 60 is the d60 grain size of the whole sample (i.e., cobble size indicator)

all 60/10 is d60 divided by d10 for the whole sample (i.e, sorting indicator)

m 10 is the d10 grain size of matrix grains (<9.525 mm)

m 60/10 is d60 divided by d10 for the matrix fraction (i.e, sorting indicator)

% cobbles is the solid volume fraction larger than 9.525 mm (i.e., framework proportion indicator)

Table S4B. Eigenvectors

	Eigenvector 1	Eigenvector 2	Eigenvector 3	Eigenvector 4	Eigenvector 5	Eigenvector 6	Eigenvector 7	Eigenvector 8
K (skin 5E-4)	0.125	0.255	-0.345	-0.213	0.426	-0.518	0.543	-0.103
m porosity	-0.177	-0.581	-0.462	0.319	0.0652	0.161	0.327	0.423
CC	-0.0358	-0.0612	0.478	0.272	-0.495	-0.194	0.629	-0.119
all 60	-0.645	0.528	-0.0650	-0.0922	-0.205	-0.0630	0.0170	0.496
all 60/10	0.245	-0.337	-0.0655	-0.502	-0.441	-0.477	-0.182	0.338
m 10	-0.0738	-0.0216	-0.196	-0.621	-0.244	0.571	0.347	-0.254
m 60/10	-0.0450	-0.197	0.624	-0.336	0.510	0.128	0.164	0.392
% cobbles	0.684	0.403	-0.0493	0.139	-0.115	0.307	0.148	0.467

Table S4C. Eigenvalues

	1	2	3	4	5	6	7	8
1	0.0599							
2		0.131						
3			0.312					
4				0.408				
5					0.807			
6						1.116		
7							1.532	
8								3.634

Table S5A. Variance-Covariance Matrix

	K (skin 5E-4)	m porosity	CC	all 60	all 60/10	m 10	m 60/10	% cobbles
K (skin 5E-4)	1	0.108	0.134	0.0973	0.171	-0.046	-0.429	-0.0840
m porosity	0.108	1	0.00511	0.763	0.438	-0.322	0.251	0.825
CC	0.134	0.00511	1	-0.148	-0.0447	-0.241	-0.0184	-0.0475
all 60	0.0973	0.763	-0.148	1	0.725	-0.381	0.0331	0.808
all 60/10	0.171	0.438	-0.0447	0.725	1	-0.664	-0.0898	0.541
m 10	-0.0460	-0.322	-0.241	-0.381	-0.664	1	-0.0495	-0.416
m 60/10	-0.429	0.251	-0.0184	0.0331	-0.0898	-0.0495	1	0.402
% cobbles	-0.0840	0.825	-0.0475	0.808	0.541	-0.416	0.402	1

K (skin 5E-4) is log10K calculated from slug tests with a wellbore skin value of 5E-4m/s

m porosity is sample porosity assigned to matrix volume

CC is capacitive conductivity

all 60 is the d60 grain size of the whole sample (i.e., cobble size indicator)

all 60/10 is d60 divided by d10 for the whole sample (i.e, sorting indicator)

m 10 is the d10 grain size of matrix grains (<9.525 mm)

m 60/10 is d60 divided by d10 for the matrix fraction (i.e, sorting indicator)

% cobbles is the solid volume fraction larger than 9.525 mm (i.e., framework proportion indicator)

Table S5B. Eigenvectors

	Eigenvector 1	Eigenvector 2	Eigenvector 3	Eigenvector 4	Eigenvector 5	Eigenvector 6	Eigenvector 7	Eigenvector 8
K (skin 5E-4)	-0.0364	0.129	0.0645	-0.588	-0.487	0.139	-0.611	0.0378
m porosity	0.116	-0.602	-0.447	0.120	-0.435	0.0652	0.0930	0.455
CC	-0.0173	-0.00834	0.255	0.345	-0.339	-0.808	-0.220	-0.0115
all 60	-0.725	0.156	0.254	0.286	-0.0517	0.243	-0.0458	0.490
all 60/10	0.367	-0.366	0.547	-0.0781	0.415	0.027	-0.265	0.428
m 10	0.212	-0.120	0.525	0.290	-0.482	0.438	0.201	-0.339
m 60/10	-0.192	-0.117	0.301	-0.586	-0.139	-0.268	0.640	0.119
% cobbles	0.493	0.659	-0.0246	0.0670	-0.177	0.0117	0.217	0.489

Table S5C. Eigenvalues

	1	2	3	4	5	6	7	8
1	0.0829							
2		0.126						
3			0.267					
4				0.479				
5					0.857			
6						1.148		
7							1.608	
8								3.432

Table S6A. Variance-Covariance Matrix

	K (skin 5E-4)	m porosity	CC	all 60	all 60/10	m 10	m 60/10	% cobbles
K (skin 5E-4)	1	0.479	-0.406	-0.182	-0.138	-0.0992	0.0977	0.0198
m porosity	0.479	1	-0.411	0.281	0.268	-0.111	-0.140	0.470
CC	-0.406	-0.411	1	-0.227	-0.298	0.263	0.175	-0.320
all 60	-0.182	0.281	-0.227	1	0.862	-0.235	-0.157	0.852
all 60/10	-0.138	0.268	-0.298	0.862	1	-0.516	-0.279	0.773
m 10	-0.0992	-0.111	0.263	-0.235	-0.516	1	-0.0315	-0.216
m 60/10	0.0977	-0.140	0.175	-0.157	-0.279	-0.0315	1	-0.147
% cobbles	0.0198	0.470	-0.320	0.852	0.773	-0.216	-0.147	1

K (skin 5E-4) is log10K calculated from slug tests with a wellbore skin value of 5E-4m/s

m porosity is sample porosity assigned to matrix volume

CC is capacitive conductivity

all 60 is the d60 grain size of the whole sample (i.e., cobble size indicator)

all 60/10 is d60 divided by d10 for the whole sample (i.e, sorting indicator)

m 10 is the d10 grain size of matrix grains (<9.525 mm)

m 60/10 is d60 divided by d10 for the matrix fraction (i.e, sorting indicator)

% cobbles is the solid volume fraction larger than 9.525 mm (i.e., framework proportion indicator)

Table S6B. Eigenvectors

	Eigenvector 1	Eigenvector 2	Eigenvector 3	Eigenvector 4	Eigenvector 5	Eigenvector 6	Eigenvector 7	Eigenvector 8
K (skin 5E-4)	-0.0159	-0.0891	0.694	-0.156	-0.0683	-0.0718	-0.687	0.0577
m porosity	0.00679	-0.155	-0.596	-0.453	-0.280	0.206	-0.447	0.309
CC	-0.00214	0.00453	0.238	-0.769	-0.292	-0.0425	0.423	-0.293
all 60	-0.651	-0.407	0.169	0.118	-0.252	0.00313	0.277	0.478
all 60/10	0.701	-0.393	0.147	-0.0545	0.109	-0.101	0.238	0.501
m 10	0.249	-0.186	0.122	0.329	-0.555	0.636	0.0335	-0.260
m 60/10	0.126	-0.0913	-0.154	0.229	-0.577	-0.731	-0.0790	-0.162
% cobbles	0.0871	0.778	0.133	0.0357	-0.339	0.0493	0.0937	0.492

Table S6C. Eigenvalues

	1	2	3	4	5	6	7	8
1	0.0691							
2		0.134						
3			0.341					
4				0.539				
5					0.900			
6						1.058		
7							1.696	
8								3.264

Table S7A. Variance-Covariance Matrix

	K (skin 5E-4)	m porosity	CC	all 60	all 60/10	m 10	m 60/10	% cobbles
K (skin 5E-4)	1	0.199	-0.202	0.242	0.213	0.0401	-0.223	0.0068
m porosity	0.199	1	-0.105	0.533	0.122	-0.0748	-0.0003	0.747
CC	-0.202	-0.105	1	-0.0224	0.235	-0.345	0.170	-0.0304
all 60	0.242	0.533	-0.0224	1	0.676	-0.198	-0.297	0.735
all 60/10	0.213	0.122	0.235	0.676	1	-0.601	-0.498	0.297
m 10	0.0401	-0.0748	-0.345	-0.198	-0.601	1	0.0289	-0.199
m 60/10	-0.223	-0.0003	0.170	-0.297	-0.498	0.0289	1	0.0610
% cobbles	0.0068	0.747	-0.0304	0.735	0.297	-0.199	0.0610	1

K (skin 5E-4) is log10K calculated from slug tests with a wellbore skin value of 5E-4m/s

m porosity is sample porosity assigned to matrix volume

CC is capacitive conductivity

all 60 is the d60 grain size of the whole sample (i.e., cobble size indicator)

all 60/10 is d60 divided by d10 for the whole sample (i.e, sorting indicator)

m 10 is the d10 grain size of matrix grains (<9.525 mm)

m 60/10 is d60 divided by d10 for the matrix fraction (i.e, sorting indicator)

% cobbles is the solid volume fraction larger than 9.525 mm (i.e., framework proportion indicator)

Table S7B. Eigenvectors

	Eigenvector 1	Eigenvector 2	Eigenvector 3	Eigenvector 4	Eigenvector 5	Eigenvector 6	Eigenvector 7	Eigenvector 8
K (skin 5E-4)	-0.0142	-0.202	0.0374	-0.0512	0.825	-0.452	0.196	0.178
m porosity	-0.0271	0.466	-0.624	-0.0353	0.108	0.267	0.396	0.388
CC	0.0584	-0.114	-0.180	-0.695	0.246	0.342	-0.538	0.0324
all 60	0.628	0.169	0.473	-0.203	-0.131	-0.0197	0.0960	0.534
all 60/10	-0.617	0.382	0.236	0.0239	-0.0530	-0.224	-0.397	0.454
m 10	-0.311	0.145	0.224	-0.660	-0.172	-0.156	0.519	-0.270
m 60/10	-0.111	0.292	0.487	0.189	0.425	0.628	0.101	-0.212
% cobbles	-0.334	-0.669	0.0994	0.0104	-0.131	0.371	0.262	0.455

Table S7C. Eigenvalues

	1	2	3	4	5	6	7	8
1	0.0662							
2		0.138						
3			0.416					
4				0.592				
5					0.790			
6						1.469		
7							1.643	
8								2.886

Supporting Information: Tables S8A to S8C with Statistics Supporting 8-way PCA for G K-facies

Table S8A. Variance-Covariance Matrix

	K (skin 5E-4)	m porosity	CC	all 60	all 60/10	m 10	m 60/10	% cobbles
K (skin 5E-4)	1	0.160	-0.434	0.456	0.443	-0.3484	-0.216	0.304
m porosity	0.160	1	0.0885	0.781	0.687	-0.415	-0.363	0.826
CC	-0.434	0.0885	1	-0.052	-0.199	0.249	-0.157	0.144
all 60	0.456	0.781	-0.052	1	0.788	-0.516	-0.314	0.836
all 60/10	0.443	0.687	-0.199	0.788	1	-0.760	-0.057	0.709
m 10	-0.3484	-0.415	0.249	-0.516	-0.760	1	-0.224	-0.426
m 60/10	-0.216	-0.363	-0.157	-0.314	-0.057	-0.224	1	-0.316
% cobbles	0.304	0.826	0.144	0.836	0.709	-0.426	-0.316	1

K (skin 5E-4) is log10K calculated from slug tests with a wellbore skin value of 5E-4m/s

m porosity is sample porosity assigned to matrix volume

CC is capacitive conductivity

all 60 is the d60 grain size of the whole sample (i.e., cobble size indicator)

all 60/10 is d60 divided by d10 for the whole sample (i.e, sorting indicator)

m 10 is the d10 grain size of matrix grains (<9.525 mm)

m 60/10 is d60 divided by d10 for the matrix fraction (i.e, sorting indicator)

% cobbles is the solid volume fraction larger than 9.525 mm (i.e., framework proportion indicator)

Table S8B. Eigenvectors

	Eigenvector 1	Eigenvector 2	Eigenvector 3	Eigenvector 4	Eigenvector 5	Eigenvector 6	Eigenvector 7	Eigenvector 8
K (skin 5E-4)	0.1146	0.174	-0.2880	0.197	-0.591	-0.554	-0.330	0.263
m porosity	0.3939	0.351	-0.548	0.0485	0.3995	0.108	0.266	0.421
CC	0.1061	0.157	0.002	-0.086	-0.6690	0.358	0.614	-0.063
all 60	0.517	-0.285	0.603	0.253	-0.0007	-0.035	0.085	0.465
all 60/10	-0.411	0.6278	0.396	-0.1499	0.000	0.163	-0.1606	0.453
m 10	-0.109	0.383	0.200	0.628	0.176	-0.352	0.370	-0.340
m 60/10	0.1262	0.096	-0.0881	0.570	-0.108	0.6282	-0.464	-0.144
% cobbles	-0.5968	-0.436	-0.222	0.383	-0.024	0.0826	0.2402	0.439

Table S8C. Eigenvalues

	1	2	3	4	5	6	7	8
1	0.1250							
2		0.1334						
3			0.156					
4				0.334				
5					0.478			
6						1.125		
7							1.642	
8								4.006

Supporting Information: Tables S9A to S9C with Statistics Supporting 8-way PCA for H K-facies

Table S9A. Variance-Covariance Matrix

	K (skin 5E-4)	m porosity	CC	all 60	all 60/10	m 10	m 60/10	% cobbles
K (skin 5E-4)	1	0.136	-0.020	-0.046	-0.148	0.2898	-0.209	-0.163
m porosity	0.136	1	0.1712	0.202	0.137	0.207	0.274	0.259
CC	-0.020	0.1712	1	-0.637	-0.644	0.594	-0.506	-0.698
all 60	-0.046	0.202	-0.637	1	0.898	-0.566	0.761	0.805
all 60/10	-0.148	0.137	-0.644	0.898	1	-0.622	0.773	0.813
m 10	0.2898	0.207	0.594	-0.566	-0.622	1	-0.617	-0.511
m 60/10	-0.209	0.274	-0.506	0.761	0.773	-0.617	1	0.815
% cobbles	-0.163	0.259	-0.698	0.805	0.813	-0.511	0.815	1

K (skin 5E-4) is log10K calculated from slug tests with a wellbore skin value of 5E-4m/s

m porosity is sample porosity assigned to matrix volume

CC is capacitive conductivity

all 60 is the d60 grain size of the whole sample (i.e., cobble size indicator)

all 60/10 is d60 divided by d10 for the whole sample (i.e, sorting indicator)

m 10 is the d10 grain size of matrix grains (<9.525 mm)

m 60/10 is d60 divided by d10 for the matrix fraction (i.e, sorting indicator)

% cobbles is the solid volume fraction larger than 9.525 mm (i.e., framework proportion indicator)

Table S9B. Eigenvectors

	Eigenvector 1	Eigenvector 2	Eigenvector 3	Eigenvector 4	Eigenvector 5	Eigenvector 6	Eigenvector 7	Eigenvector 8
K (skin 5E-4)	-0.0466	0.133	-0.1670	-0.022	0.316	-0.819	0.415	-0.094
m porosity	0.0902	-0.033	0.394	0.3676	0.0954	0.317	0.766	0.064
CC	-0.3121	0.280	-0.214	-0.491	0.4328	0.426	0.194	-0.361
all 60	-0.421	-0.554	0.245	-0.495	-0.0037	-0.084	0.136	0.430
all 60/10	0.531	0.4852	0.225	-0.4870	-0.013	-0.015	0.0470	0.438
m 10	0.210	-0.165	-0.273	-0.321	-0.695	-0.009	0.382	-0.350
m 60/10	0.3142	-0.305	-0.7099	0.083	0.266	0.1942	0.127	0.416
% cobbles	-0.5387	0.490	-0.286	0.178	-0.387	0.0372	0.1424	0.430

Table S9C. Eigenvalues

	1	2	3	4	5	6	7	8
1	0.0894							
2		0.0981						
3			0.228					
4				0.317				
5					0.407			
6						1.010		
7							1.358	
8								4.493
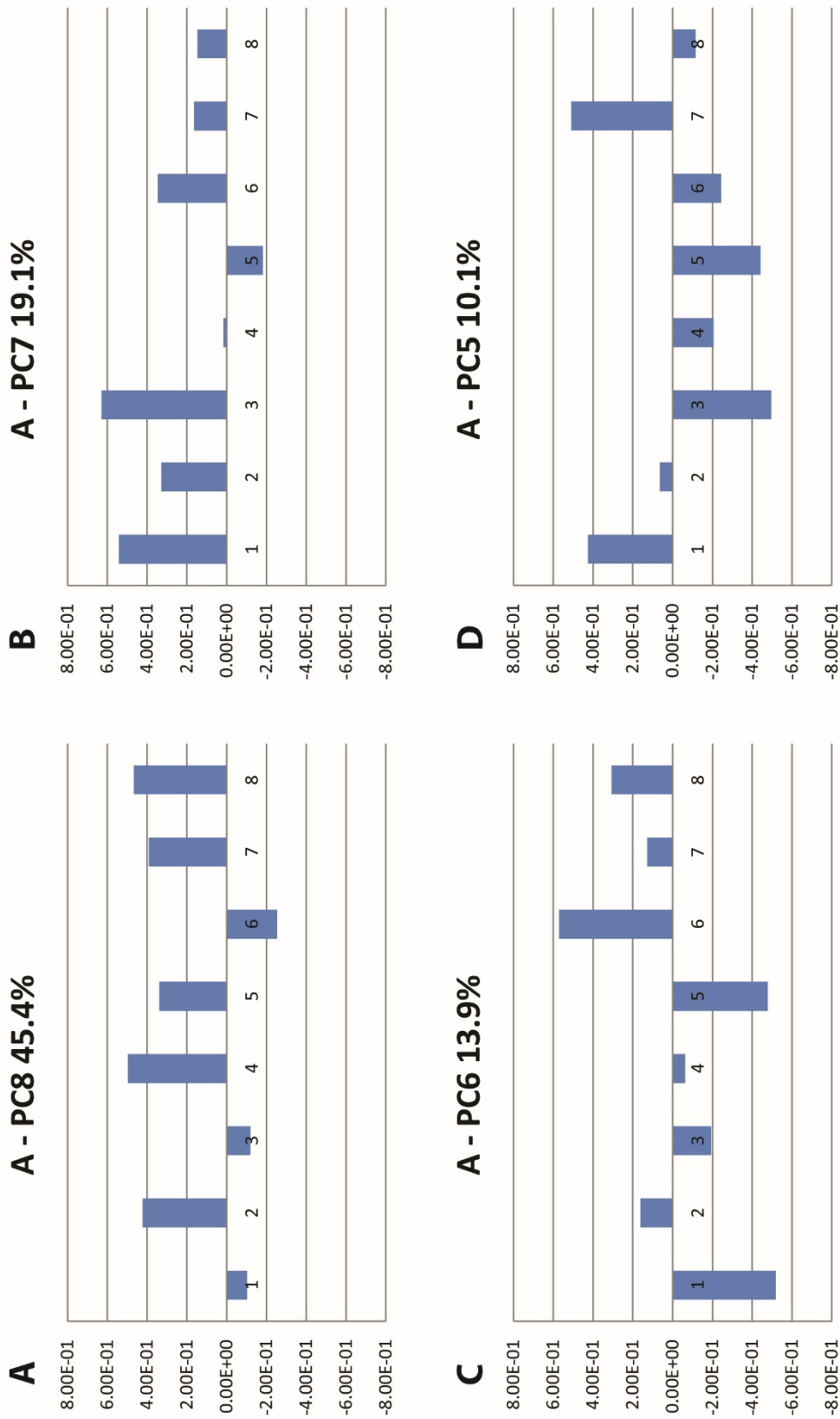
Figure S1. Four eigenvectors explain 88.5% of system variance of K-facies A (Unit1) for 8-way PCA that includes grain-size and matrix vs framework parameters. Eight parameters are: 1=log10K (m/s); 2=porosity assigned to matrix; 3=CC or capacitive conductivity (mS/m); 4=d60 of the full sample GSD; 5=d60/d10 of the full sample GSD; 6=d10 of the matrix fraction; 7=d60/d10 of the matrix fraction; 8=volume fraction of grains >9.525mm. A. PC8 indicates >45% of system variance is associated with cobble size and volume fraction. B. In PC7, CC varies especially with K, matrix porosity, and matrix d10. C. In PC6, K varies especially in opposition to full GSD sorting quality (i.e., low sorting is well-sorted), matrix d10, and volume of cobbles. D. In PC5, K varies especially in opposition to CC and matrix sorting, and varies with full sample sorting quality.
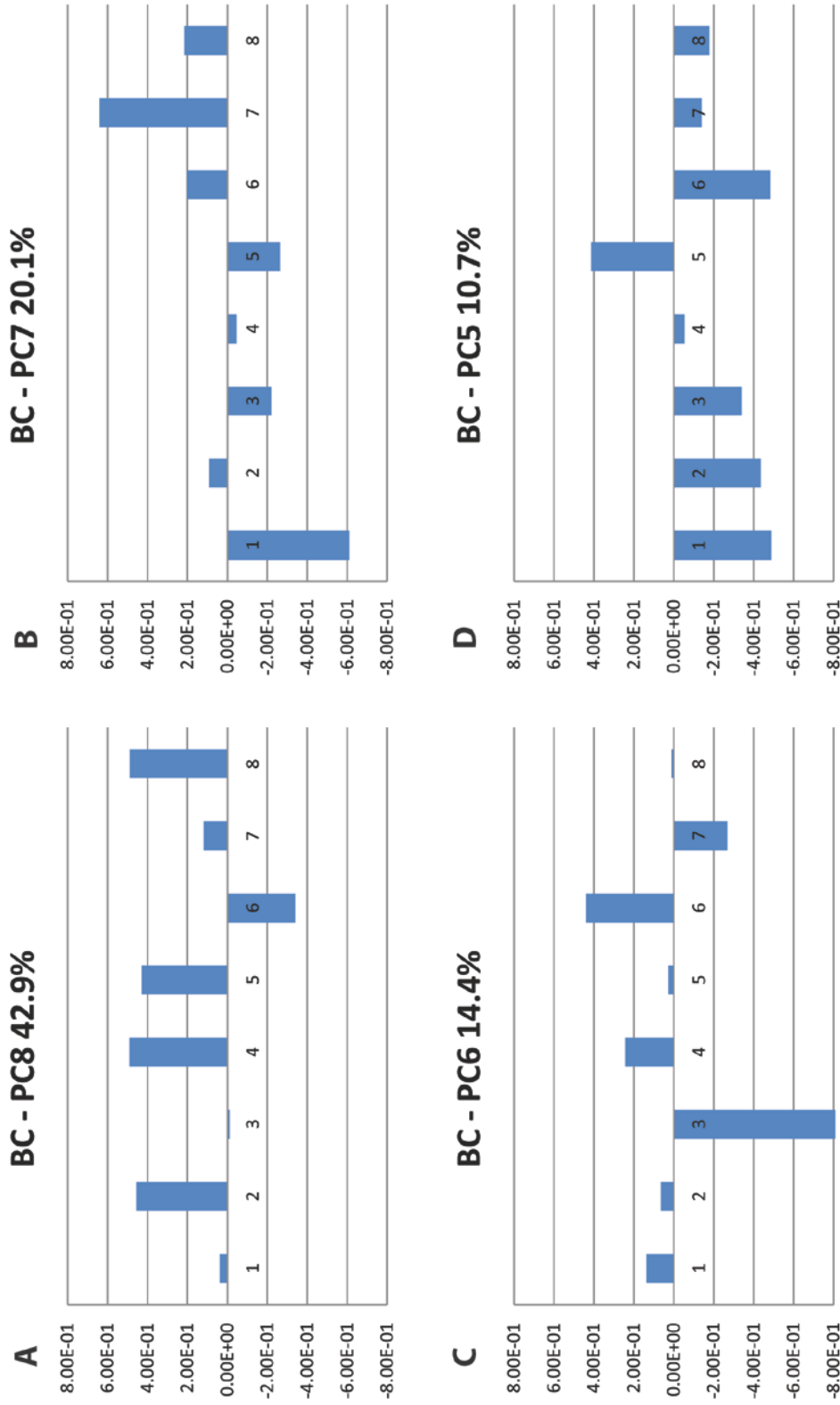
Figure S2. Four eigenvectors explain 88.1% of system variance of K-facies BC for 8-way PCA that includes grain-size and matrix vs framework parameters. Eight parameters are: 1=log10K (m/s); 2=porosity assigned to matrix; 3=CC or capacitive conductivity (mS/m); 4=d60 of the full sample GSD; 5=d60/d10 of the full sample GSD; 6=d10 of the matrix fraction; 7=d60/d10 of the matrix fraction; 8=volume fraction of grains >9.525mm. A. In PC8, 42.9% of system variance is largely associated with cobble size, sorting, and volume fraction. B. In PC7, K varies especially with matrix sorting and in opposition to d10m and cobble volume fraction. C. PC6 is dominated by CC which is in opposition to cobble size, d10m, and quality of matix sorting (i.e, lower d60/d10 is better sorting). D. In PC5, K, matrix porosity, and CC vary together with d10m and cobble volume fraction, and quality of full sample sorting.
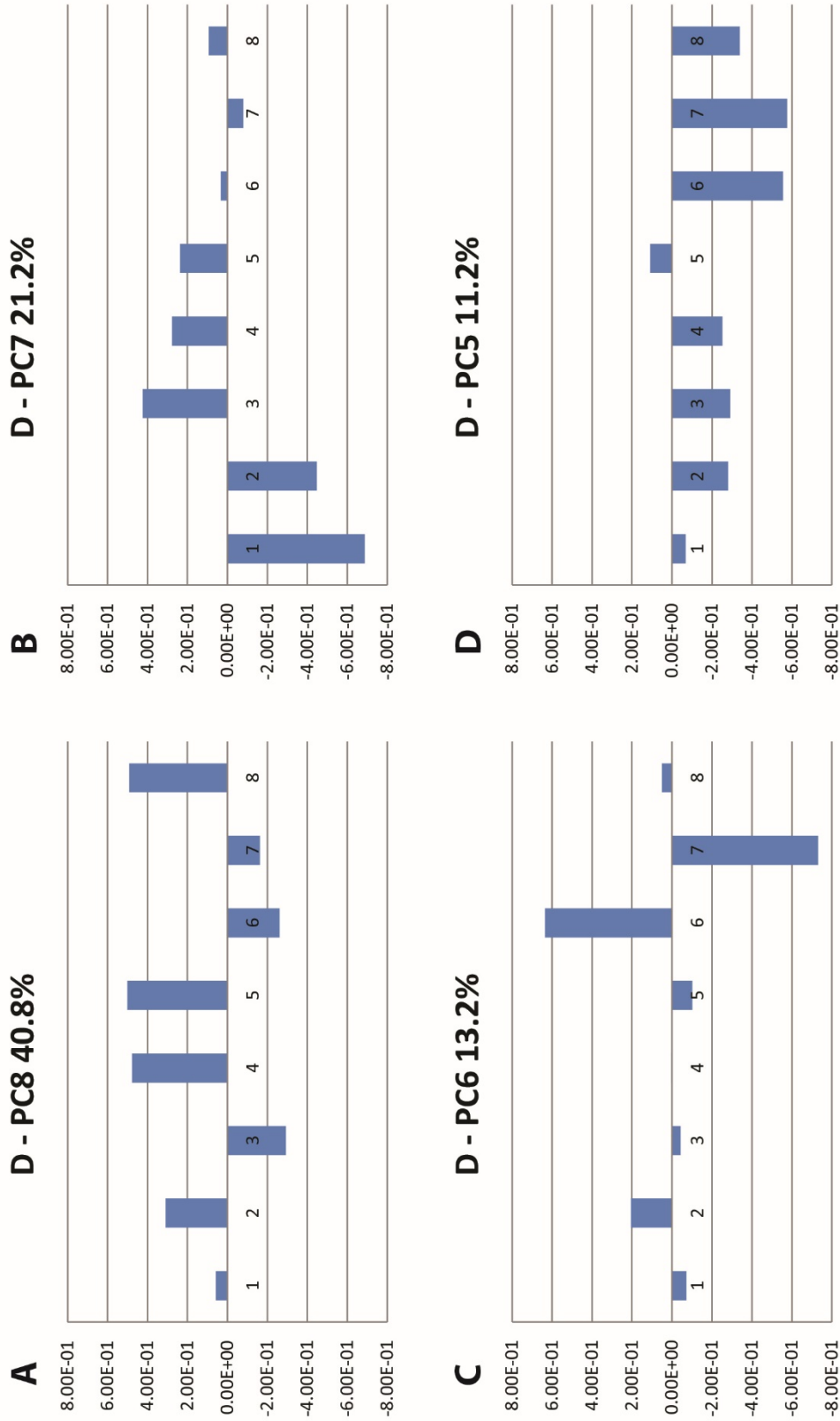
Figure S3. Four eigenvectors explain 86.4% of system variance of K-facies D for 8-way PCA that includes grain-size and matrix vs framework parameters. Eight parameters are: 1=log10K (m/s); 2=porosity assigned to matrix; 3=CC or capacitive conductivity (mS/m); 4=d60 of the full sample GSD; 5=d60/d10 of the full sample GSD; 6=d10 of the matrix fraction; 7=d60/d10 of the matrix fraction; 8=volume fraction of grains >9.525mm. A. PC8 indicates 40.8% of system variance is largely associated with cobble size, sorting, and volume fraction. B. In PC7 (only PC with significant K), K varies with matrix porosity and sample sorting quality (i.e., lower d60/d10 is better sorting), and in opposition to CC and cobble size. C. PC6 is dominated by matrix d10 and matrix sorting quality. D. In PC5, matrix porosity and CC vary with cobble size, cobble volume fraction, and d10m, but vary in opposition to matrix sorting quality.
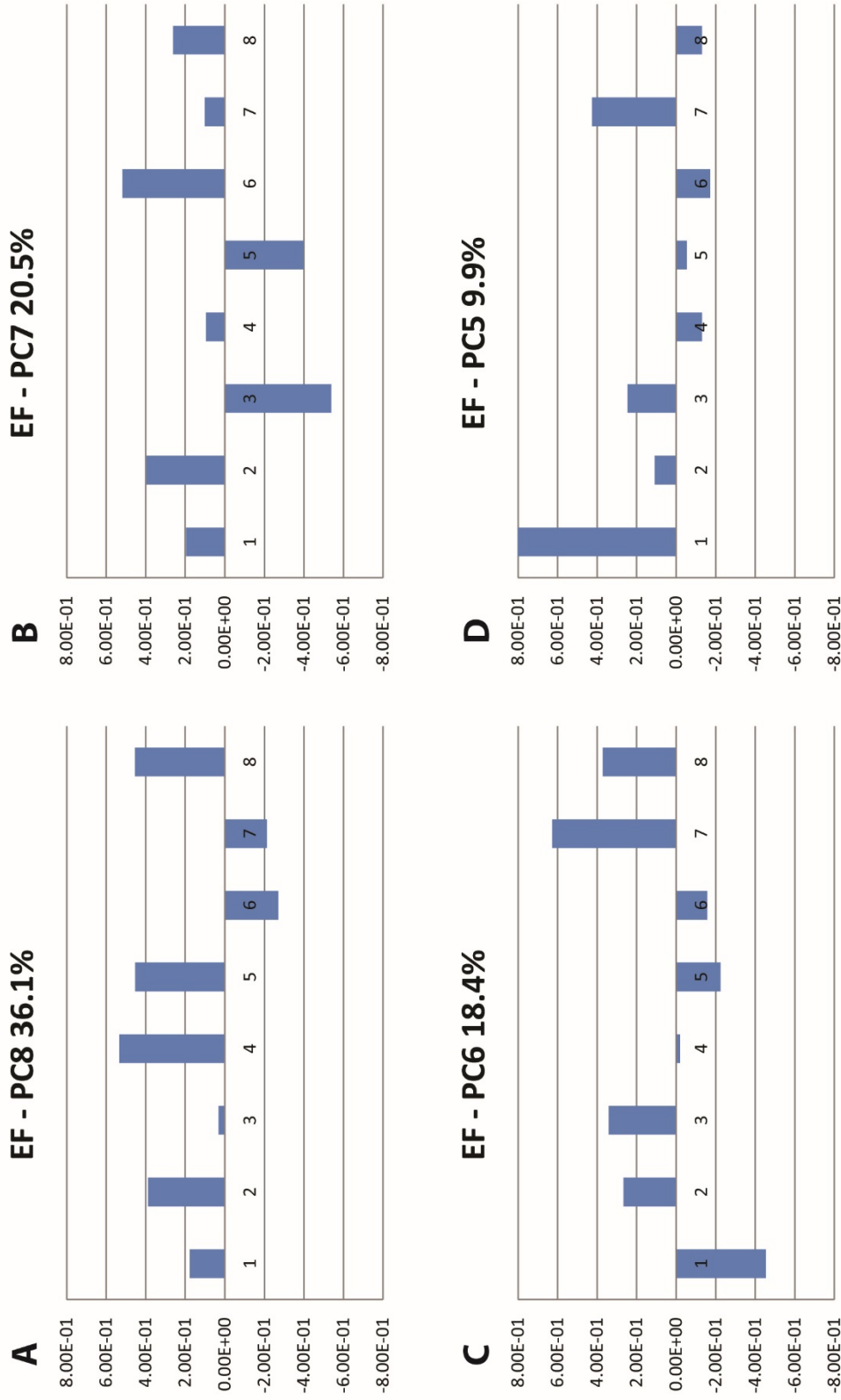
Figure S4. Four eigenvectors explain 84.9% of system variance of K-facies EF for 8-way PCA that includes grain-size and matrix vs framework parameters. Eight parameters are: 1=log10K (m/s); 2=porosity assigned to matrix; 3=CC or capacitive conductivity (mS/m); 4=d60 of the full sample GSD; 5=d60/d10 of the full sample GSD; 6=d10 of the matrix fraction; 7=d60/d10 of the matrix fraction; 8=volume fraction of grains >9.525mm. A. PC8 indicates 36.1% of system variance is largely associated with cobble size, sorting, and volume fraction. B. In PC7, K, matrix porosity, matrix d10, sample sorting quality (i.e., lower d60/d10 is better sorting), and cobble volume fraction vary together but in opposition to CC. C. In PC6, K varies with matrix sorting quality and in opposition to matrix porosity, CC, and copbble volume fraction. D. In PC5, K dominates and varies with CC and in opposition to matrix sorting quality.

68
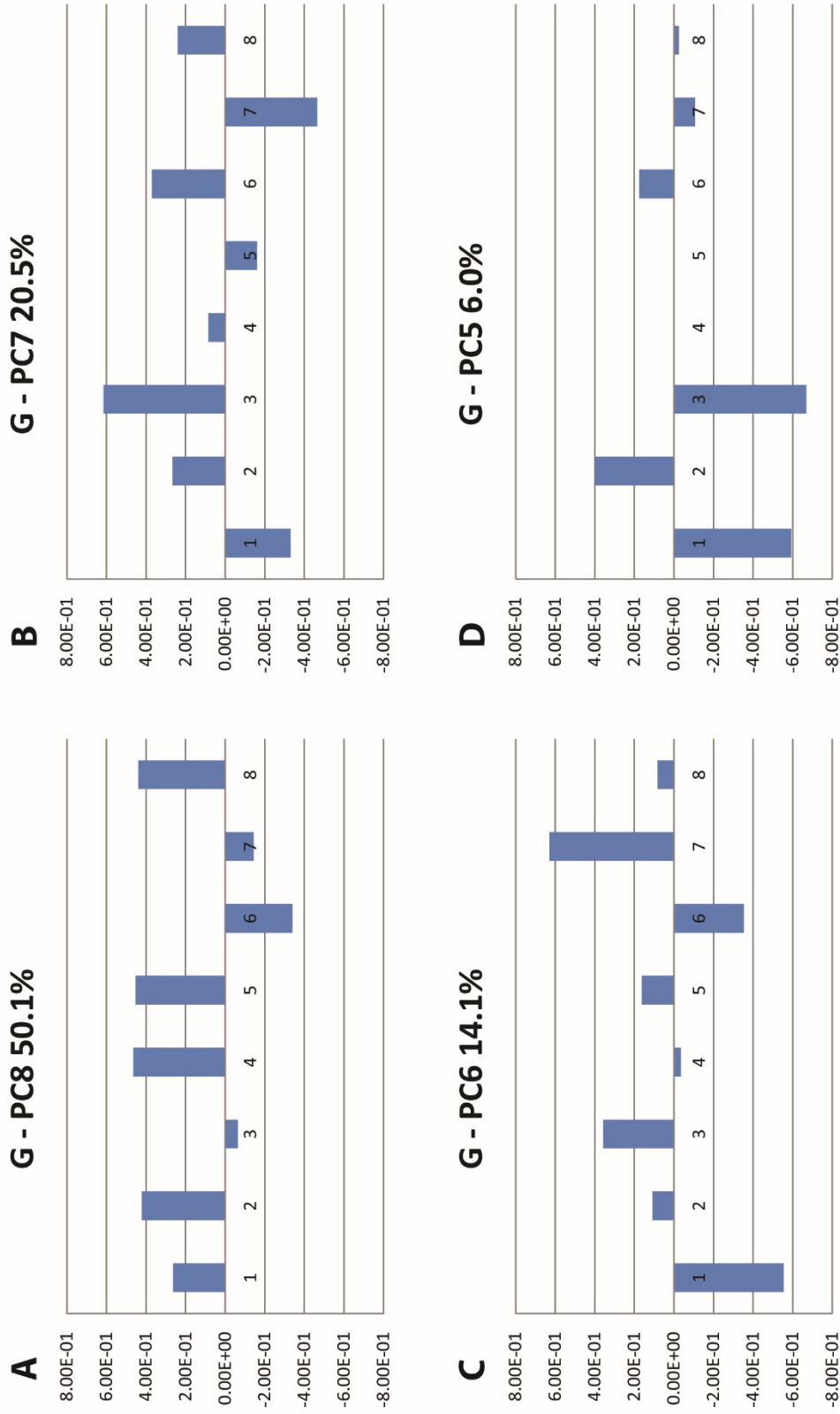
Figure S5. Four eigenvectors explain 90.7% of system variance of K-facies G for 8-way PCA that includes grain-size and matrix vs framework parameters. Eight parameters are: 1=log10K (m/s); 2=porosity assigned to matrix; 3=CC or capacitive conductivity (mS/m); 4=d60 of the full sample GSD; 5=d60/d10 of the full sample GSD; 6=d10 of the matrix fraction; 7=d60/d10 of the matrix fraction; 8=volume fraction of grains >9.525mm. A. PC8 indicates 50.1% of system variance is associated with K and matrix porosity varying together with cobble size and volume fraction, but in opposition to d10m and sample sorting quality (i.e., lower d60/d10 is better sorting). B and C. PC7 and PC6 are largely similar except for opposite contributions from d10m and matrix sorting quality. D. In PC5, K varies with CC but in opposition to matrix porosity, d10m, and matrix sorting quality.

69
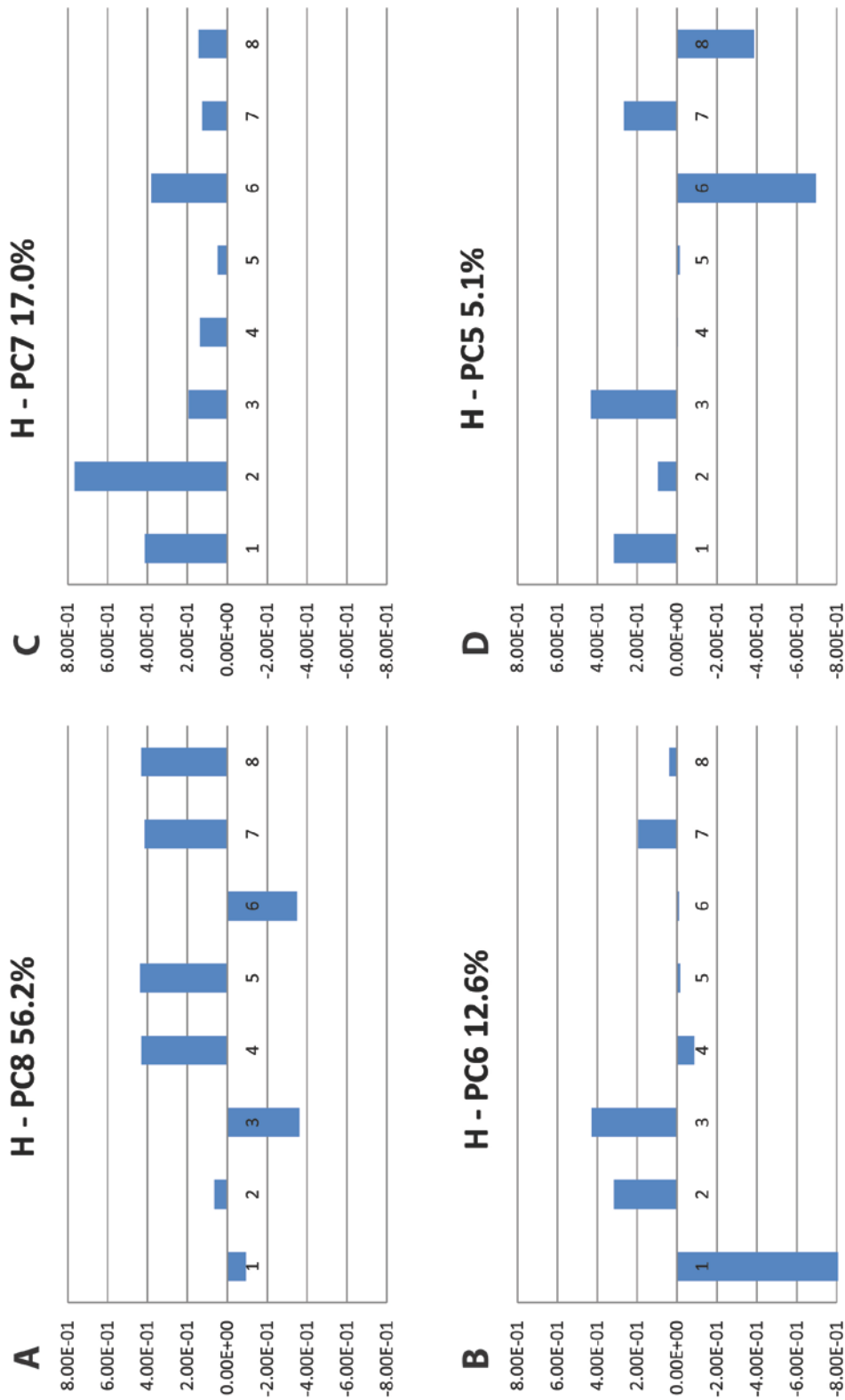
Figure S6. Four eigenvectors explain 90.9% of system variance of K-facies H for 8-way PCA that includes grain-size and matrix vs framework parameters. Eight parameters are: 1=log10K (m/s); 2=porosity assigned to matrix; 3=CC or capacitive conductivity (mS/m); 4=d60 of the full sample GSD; 5=d60/d10 of the full sample GSD; 6=d10 of the matrix fraction; 7=d60/d10 of the matrix fraction; 8=volume fraction of grains >9.525mm. A. PC8 indicates 56.2% of system variance is largely associated with cobble size, sorting, and volume fraction. B. PC7 is dominated by K, matrix porosity, and d10m varying together. C. PC6 is dominated by very strong contribution of K that varies with matrix sorting quality (i.e., lower d60/d10 is better sorting i and in opposition to matrix porosity and CC.. D. In PC5, K varies especially with CC and poor matrix sorting, and in opposition to d10m and cobble volume fraction.